J. Fluid Mech. (1998), *vol.* 367, *pp.* 329–358. Printed in the United Kingdom

Oscillatory motions of circular disks and nearly spherical particles in viscous flows

By WENDY ZHANG AND H. A. STONE

Division of Engineering and Applied Sciences,
Harvard University, Cambridge, MA 02138, USA

(Received 1 October 1996 and in revised form 12 March 1998)

Oscillatory translational and rotational motions of small particles in viscous fluids are studied for two cases: (i) circular disks and (ii) nearly spherical particles. For circular disks, four motions are treated: broadside and edgewise oscillatory translations and out-of-plane and in-plane oscillatory rotations. In each case the unsteady Stokes equations are reduced to dual integral equations and solved exactly for all frequencies. Streamline portraits of the flow fields are used to understand the evolution of the velocity and pressure fields. The motions of nearly spherical particles are then studied using the reciprocal theorem. Asymptotic formulae for the hydrodynamic resistance tensors are derived and discussed.

1. Introduction

For many suspension flows the trajectories and orientations of the suspended particles depend on the time-dependent forces and torques that act on the particles. Classical results for transient (e.g. oscillatory) motions of spheres and cylinders in viscous fluids are well known. Recently there has been work on translational motions of more complicated, though axisymmetric, particles, such as spheroids, finite-length cylinders, and dumbbells, in an effort to elucidate the relation between the particle geometry and the hydrodynamic resistance. Here we take a more general view by considering translational and rotational motions of two distinct geometries: a circular disk and an arbitrarily shaped, though nearly spherical, particle.

Particle motions for the transient flows mentioned above are often treated within the unsteady Stokes flow approximation which retains the local acceleration of the fluid while neglecting the convective acceleration. In this low-Reynolds-number flow limit, it is sufficient to consider independent Fourier modes of the time-dependent motion. For a single oscillation frequency ω, the flow field and the corresponding hydrodynamic resistance for a particle with characteristic dimension a, in a fluid with kinematic viscosity ν, depend only on the dimensionless frequency parameter $\lambda^2 = \omega a^2/\nu$ and the detailed particle shape. Analytical results are available for a sphere or a cylinder undergoing oscillatory translational or rotational motion (e.g. Stokes 1851), but exact results at arbitrary λ^2 for other geometries are few.

Lawrence & Weinbaum (1986, 1988) developed an exact solution for arbitrary λ^2 for the axisymmetric translation of a spheroid. Their analytical solution showed that the time-dependent force on the oscillating particle consisted of the familiar steady Stokes drag, the added mass, and the Basset history force, in addition to a new memory term due to the particle's non-spherical shape. Lawrence & Weinbaum (1988) reported results for axisymmetric translational motions for spheroids with aspect

ratios 0.1–10. These studies were extended by Pozrikidis who developed a singularity solution method to investigate axial and transverse oscillations of prolate spheroids (1989*a*) and a boundary integral representation to study axisymmetric oscillatory flow past spheroids, dumbbell-shaped particles and biconcave disks (1989*b*). Loewenberg (1993*a*, *b*, 1994*a*, *b*) used the boundary integral procedure to study the transverse and axial oscillations of finite-length cylinders and spheroids. We also note that Davis (1993*b*) studied the hydrodynamics of an oscillating screen viscometer in which the oscillations of a periodic rectangular grid were analysed as were the broadside oscillations of a thin annular disk. Rotational oscillations have received much less attention. Series solutions for rotational motions of a spheroid were developed by Hocquart (1976, 1977) but no results were reported.

Generally, unsteady Stokes flow problems arise in situations such as the calibration of electroacoustic measurements (Loewenberg 1994*c*), as well as more well-known problems on Brownian motion and swimming microorganisms. Some biological applications are mentioned by Vogel (1994). Also, the use of high-frequency torsional oscillations of a circular disk as a device for measuring viscosity has a long history (e.g. Faber 1995). In recent years a new engineering application has appeared to which some of the unsteady viscous flow ideas apply (e.g. Bryzek, Peterson & McCulley 1994): silicon processing technology has been used to construct microelectromechanical systems which include a variety of small mechanical elements such as gears, levers, valves, and microactuators that operate in time-periodic or other transient modes. The performance of such mechanisms, which are often less than 100 μm in size, may be significantly affected by viscous dissipation in the surrounding fluid. At typical frequencies of operation, the fluid motion is often characterized by a Reynolds number about 1, but may encompass a wide range of λ^2. The effect on the mechanical element, or particle, of nearby rigid boundaries is frequently important as are finite Knudsen number effects owing to the mean free path of the fluid becoming comparable to the geometric dimensions (e.g. Arkilic, Schmidt & Breuer 1995). These latter effects are not considered in this paper, but in some cases can be treated within the mathematical framework described in § 2. Also, the unsteady Stokes equation has the same mathematical form as the Brinkman equation which describes steady motions in a porous medium under certain circumstances.

As summarized above the flow fields and the hydrodynamic resistance on particles in unsteady Stokes flows have been investigated primarily for spheres, cylinders and spheroids of modest aspect ratios and for translational motions. For other particle shapes, such as circular disks, some asymptotic results are available for both low and high frequencies (§ 3 and Appendix B), but exact results at arbitrary λ^2 are apparently only available for edgewise oscillatory translation of a circular disk (Davis 1993*a*); Lai's (1973) results on broadside oscillations of a circular disk are in error as the analysis begins by assuming incorrectly that the force is given by a formula equivalent to that for a sphere.

Motivated by the circular shape of some of the microelectromechanical elements discussed above, we study in §§ 2 and 3 and Appendix A time-periodic motions, and the corresponding forces and torques, on circular disk-shaped particles. The analytical development in § 2 and Appendix A gives simple formulae from which the velocity field can be constructed for four representative motions. Section 3 presents the calculated hydrodynamic resistance on an oscillating disk as well as detailed velocity fields due to broadside translations and out-of-plane rotations of the circular disk. In § 4 the case of nearly spherical particles undergoing oscillatory translations and rotations are investigated and formulae for the force and torque at arbitrary λ^2 are derived. These

formulae complement other results available in the literature for specific shapes at low or high λ^2. Coupling of translational and rotational motions is also considered, as is the hydrodynamic resistance experienced by a particle moving in a time-dependent manner. In § 5 the asymptotic results derived for near-spherical particles are used as a guide in writing down a composite expansion for the hydrodynamic resistance on an oscillating disk. Comparison with the hydrodynamic resistance calculated in § 3 showed that the composite expansion is accurate when the disk motion does not displace surrounding fluid.

2. Oscillatory motions of a circular disk

2.1. *Governing equations and boundary conditions*

Consider a circular disk of radius a oscillating with frequency ω in an unbounded region filled with a fluid of viscosity μ, density ρ and kinematic viscosity $\nu = \mu/\rho$. The disk motion may be an oscillatory translation with velocity $\boldsymbol{U}\cos\omega t$, an oscillatory rotation with angular velocity $\boldsymbol{\Omega}\cos\omega t$, or a combination of rotational and translational oscillations. Non-dimensionalizing lengths by a, velocities by $u_c = |\boldsymbol{U}|$ or $u_c = |\boldsymbol{\Omega}|a$, and time by ω^{-1} yields the dimensionless Navier–Stokes and continuity equations

$$\lambda^2\frac{\partial \boldsymbol{u}}{\partial t} + \mathscr{R}\boldsymbol{u}\cdot\nabla\boldsymbol{u} = -\nabla p + \nabla^2\boldsymbol{u} \quad \text{and} \quad \nabla\cdot\boldsymbol{u} = 0, \tag{1}$$

where $\lambda^2 = \omega a^2/\nu$ and the Reynolds number $\mathscr{R} = au_c/\nu$. The dimensionless frequency parameter λ^2 characterizes the time scale for vorticity diffusion into the surrounding fluid relative to the oscillation time scale.

The momentum equation may be linearized in the limit $\mathscr{R} \ll 1$ (e.g. Batchelor 1967; Landau & Lifshitz 1959). Provided the oscillations have an amplitude u_c/ω that is smaller than the particle radius a, i.e. $\lambda^2 \gg \mathscr{R}$, equation (1) may be simplified to the unsteady Stokes equation

$$\lambda^2\frac{\partial \boldsymbol{u}}{\partial t} = -\nabla p + \nabla^2\boldsymbol{u}. \tag{2}$$

Owing to the linearity of (2), arbitrary motions may be studied by appropriate Fourier superposition of the solution for individual frequencies. For a given frequency, we write the velocity and pressure fields as $\boldsymbol{u} = \mathrm{Re}(\boldsymbol{w}\mathrm{e}^{\mathrm{i}t})$ and $p = \mathrm{Re}(Q\mathrm{e}^{\mathrm{i}t})$, which reduces (2) to

$$\mathrm{i}\lambda^2\boldsymbol{w} = -\nabla Q + \nabla^2\boldsymbol{w} \quad \text{and} \quad \nabla\cdot\boldsymbol{w} = 0. \tag{3}$$

Note that we have defined the dimensionless frequency λ^2 to be real, whereas it is common to find the parameter to be defined with an additional factor of i. Also, we have written the complex time dependence as $\mathrm{e}^{\mathrm{i}t}$ rather than $\mathrm{e}^{-\mathrm{i}t}$ which affects some of the signs in the intermediate results reported below. The solution for a disk oscillating in an arbitrary manner can be decomposed into the four basic modes illustrated in figure 1, and will be referred to as broadside translation, edgewise translation, in-plane rotation and out-of-plane rotation.

Consistent with the linearization of the equations of motion, the coordinate system may be chosen at the disk centre. For boundary conditions, the velocity is specified on the disk and vanishes at large distances. Also, there exists a jump in the hydrodynamic stresses across the disk.

In the next section we present an analytical solution, valid for arbitrary frequencies, for out-of-plane rotational oscillations, which to our knowledge has not appeared

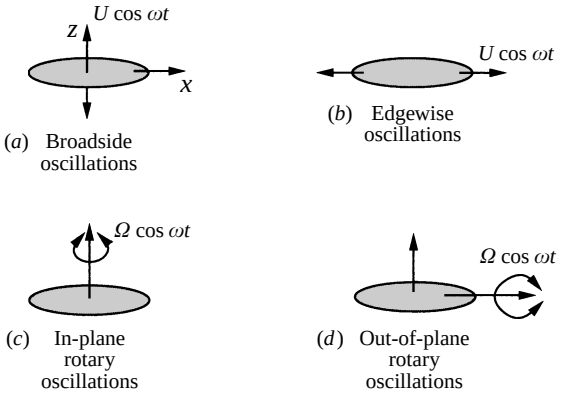

FIGURE 1. Four fundamental modes of disk oscillation.

previously in the literature. An asymptotic expression for the corresponding torque at low frequencies is derived in Appendix B. For the other three oscillation modes shown in figure 1, asymptotic results for low- and high-frequency motions are available (see § 3 and Appendix B), and for edgewise oscillations an exact solution at arbitrary λ^2 was reported recently (Davis 1993*a*). Here the same procedure may be used to obtain exact solutions for the velocity and pressure fields, as well as the hydrodynamic resistance, for all four modes of motion. The analytical details for broadside and edgewise translations and in-plane rotational oscillations of a circular disk are presented in Appendix A.

2.2. *Out-of-plane rotation of a disk*

We use a cylindrical coordinate system with the origin fixed at the centre of the disk and the z-axis normal to the disk surface. Consider out-of-plane rotation about the x-axis with angular velocity $\boldsymbol{e}_x \cos t$ as depicted in figure 1(*d*). In the small oscillation amplitude approximation the no-slip boundary condition is applied at $z = 0$ where the velocity on the disk is $\boldsymbol{w} = (0, 0, r\sin\theta)$. We expect the fluid velocity to have the same angular dependence as the boundary forcing and so choose

$$\boldsymbol{w} = (v_r(r,z)\sin\theta, v_\theta(r,z)\cos\theta, v_z(r,z)\sin\theta) \quad \text{and} \quad Q = q(r,z)\sin\theta. \tag{4}$$

It is convenient to rewrite the governing equations (3) in terms of $v_r + v_\theta, v_r - v_\theta, v_z$, and q which leads to

$$\mathrm{i}\lambda^2(v_r+v_\theta) = -\frac{1}{r}\frac{\partial}{\partial r}(rq) + \frac{\partial}{\partial r}\left(\frac{1}{r}\frac{\partial}{\partial r}(r(v_r+v_\theta))\right) + \frac{(v_r+v_\theta)}{r^2} + \frac{\partial^2}{\partial z^2}(v_r+v_\theta), \tag{5a}$$

$$\mathrm{i}\lambda^2(v_r-v_\theta) = -r\frac{\partial}{\partial r}\left(\frac{q}{r}\right) + \frac{\partial}{\partial r}\left(\frac{1}{r}\frac{\partial}{\partial r}(r(v_r-v_\theta))\right) - \frac{3(v_r-v_\theta)}{r^2} + \frac{\partial^2}{\partial z^2}(v_r-v_\theta), \tag{5b}$$

$$\mathrm{i}\lambda^2 v_z = -\frac{\partial q}{\partial z} + \frac{1}{r}\frac{\partial}{\partial r}\left(r\frac{\partial v_z}{\partial r}\right) - \frac{v_z}{r^2} + \frac{\partial^2 v_z}{\partial z^2}, \tag{5c}$$

$$\frac{(v_r+v_\theta)}{r} - \frac{1}{r}\frac{\partial}{\partial r}(r(v_r+v_\theta)) = \frac{1}{r}\frac{\partial}{\partial r}(r(v_r-v_\theta)) + \frac{(v_r-v_\theta)}{r} + 2\frac{\partial v_z}{\partial z}. \tag{5d}$$

The in-plane velocities v_r and v_θ have been combined in order to decouple the momentum equations. The boundary conditions at $z = 0$ on and off the disk may be

cast in a simple form using symmetry properties of the flow:

$$(v_r + v_\theta) = 0,\ (v_r - v_\theta) = 0; \quad r < 1: \quad v_z = r; \quad r > 1: \quad q = 0. \tag{6}$$

Next we take Hankel transforms of the governing equations and use the notation

$$V(k,z) = \mathscr{H}_n\{v\} = \int_0^\infty rv(r,z)\ J_n(kr)\ \mathrm{d}r, \tag{7a}$$

$$v(r,z) = \mathscr{H}_n^{-1}\{V\} = \int_0^\infty kV(k,z)\ J_n(kr)\ \mathrm{d}k. \tag{7b}$$

The transformed governing equations are

$$\ell^2 \mathscr{H}_0\{v_r + v_\theta\} = -k\mathscr{H}_1\{q\} + \frac{\mathrm{d}^2}{\mathrm{d}z^2}\mathscr{H}_0\{v_r + v_\theta\}, \tag{8a}$$

$$\ell^2 \mathscr{H}_2\{v_r - v_\theta\} = k\mathscr{H}_1\{q\} + \frac{\mathrm{d}^2}{\mathrm{d}z^2}\mathscr{H}_2\{v_r - v_\theta\}, \tag{8b}$$

$$\ell^2 \mathscr{H}_1\{v_z\} = -\frac{\mathrm{d}}{\mathrm{d}z}\mathscr{H}_1\{q\} + \frac{\mathrm{d}^2}{\mathrm{d}z^2}\mathscr{H}_1\{v_z\}, \tag{8c}$$

$$k\mathscr{H}_0\{v_r + v_\theta\} = k\mathscr{H}_2\{v_r - v_\theta\} + 2\frac{\mathrm{d}}{\mathrm{d}z}\mathscr{H}_1\{v_z\}, \tag{8d}$$

where $\ell^2 = k^2 + \mathrm{i}\lambda^2$. Solving these equations, using the first boundary condition in (6), and taking inverse Hankel transforms yields the solutions for the velocity and pressure fields ($z > 0$):

$$v_r(r,z) = \frac{1}{2}\int_0^\infty kA(k)\left(\mathrm{e}^{-\ell z} - \mathrm{e}^{-kz}\right)\left[J_0(kr) - J_2(kr)\right]\ \mathrm{d}k, \tag{9a}$$

$$v_\theta(r,z) = \frac{1}{2}\int_0^\infty kA(k)\left(\mathrm{e}^{-\ell z} - \mathrm{e}^{-kz}\right)\left[J_0(kr) + J_2(kr)\right]\ \mathrm{d}k, \tag{9b}$$

$$v_z(r,z) = \int_0^\infty kA(k)\left(\mathrm{e}^{-kz} - \frac{k}{\ell}\mathrm{e}^{-\ell z}\right)J_1(kr)\,\mathrm{d}k, \tag{9c}$$

$$q(r,z) = \mathrm{i}\lambda^2\int_0^\infty A(k)J_1(kr)\mathrm{e}^{-kz}\,\mathrm{d}k, \tag{9d}$$

where the positive square root is taken for ℓ. The unknown function $A(k)$ is determined by the on- and off-disk boundary conditions (6) and so satisfies the dual integral equations

$$\int_0^\infty kA(k)\left(1 - \frac{k}{\ell}\right)J_1(kr)\,\mathrm{d}k = r, \quad r < 1, \tag{10a}$$

$$\int_0^\infty A(k)J_1(kr)\ \mathrm{d}k = 0, \quad r > 1. \tag{10b}$$

These integral equations are solved using Tranter's method (Tranter 1966; see also Tanzosh & Stone 1995). We take $A(k)$ to have the form

$$A(k) = k^{1-\beta}\sum_{m=0}^{\infty} a_m J_{1+2m+\beta}(k), \tag{11}$$

which automatically satisfies the integral condition for $r > 1$. Then, following Tranter (1966) it can be shown that the coefficients $\{a_m\}$ satisfy a linear system of equations

derived from the integral condition for $r < 1$:

$$\sum_{m=0}^{\infty} a_m \int_0^{\infty} k^{2-2\beta}\left(1-\frac{k}{\ell}\right) J_{1+2m+\beta}(k) J_{1+2n+\beta}(k)\mathrm{d}k = \frac{\delta_{0n}}{2^{\beta}\Gamma(2+\beta)}, \quad n = 0, 1, \cdots. \quad (12)$$

Here β must be chosen to ensure that the integrals are convergent but otherwise the numerical results for the $\{a_m\}$, provided a sufficient number of terms in the infinite series are retained in the calculation, are insensitive to the precise value of β used. We have set $\beta = 1/2$ to capture the behaviour of the stress singularity characteristic of the Stokes equation at the disk edge (e.g. Vedensky & Ungarish 1994). The coefficients $\{a_m\}$ are obtained by solving the linear system (12) using a standard IMSL routine (DLSACG), where the elements in the matrix are calculated using a quadrature scheme developed by Lucas (1995) for integrals involving products of Bessel functions.

The hydrodynamic torque about the axis of rotation $\mathrm{Re}\left(\mu a^3 \boldsymbol{\Omega} L \mathrm{e}^{\mathrm{i}\omega t}\right)$ is calculated by integrating the surface stress distribution over the disk surface:

$$L = -2\pi \mathrm{i}\lambda^2 \int_0^{\infty} k^{-1} A(k) J_2(k)\,\mathrm{d}k = -\frac{4(2\pi)^{1/2}}{3}\mathrm{i}\lambda^2 a_0. \quad (13)$$

Note that by choosing $\beta = 1/2$ only a_0 is required to calculate the hydrodynamic resistance. Terms in the series decay sufficiently rapidly to yield $O(10^{-4})$ accuracy in a_0 when only the first five terms in the series (11) are retained. For typical calculations reported below, ten terms in the series are retained.

3. Results for oscillatory disk motions

Having outlined the analytical approach to the problem, we now proceed to summarize the principal results for the hydrodynamic resistance as well as the detailed velocity field due to an oscillating disk. In § 3.1 we present the hydrodynamic resistance along with a discussion of its behaviour in the limit of low- and high-frequency oscillations. In § 3.2 we present velocity fields for broadside translation and out-of-plane rotation in the case that fluid inertia is of comparable importance with viscous effects ($\lambda^2 = 1$). We will see that the time evolution of the velocity fields can be understood by considering the combined effects of a vorticity boundary layer near the disk and a point force- or stresslet-driven potential flow far from the disk.

3.1. *Hydrodynamic force and torque*

Hydrodynamic resistance on a body undergoing oscillatory motions can be written as a component that varies in phase with the body motion and a component $\pi/2$ out of phase with the body motion; the out-of-phase component does not contribute to energy dissipation. Figures 2 and 3 present, respectively, the non-dimensional in-phase and out-of-phase components of the hydrodynamic resistance for all four modes of disk oscillation. The dimensionless complex numbers F and L are, respectively, related to the dimensional force and torque on the disk by $\mathrm{Re}(\mu a \boldsymbol{U} F \mathrm{e}^{\mathrm{i}\omega t})$ and $\mathrm{Re}(\mu a^3 \boldsymbol{\Omega} L \mathrm{e}^{\mathrm{i}\omega t})$. In figure 2 the results have been plotted as the difference between the in-phase hydrodynamic resistance and the Stokes resistance (F_{Stokes} and L_{Stokes} corresponding to $\lambda = 0$), normalized with respect to the Stokes resistance. In figure 3, the out-of-phase resistances are also normalized with respect to the corresponding Stokes flow values.

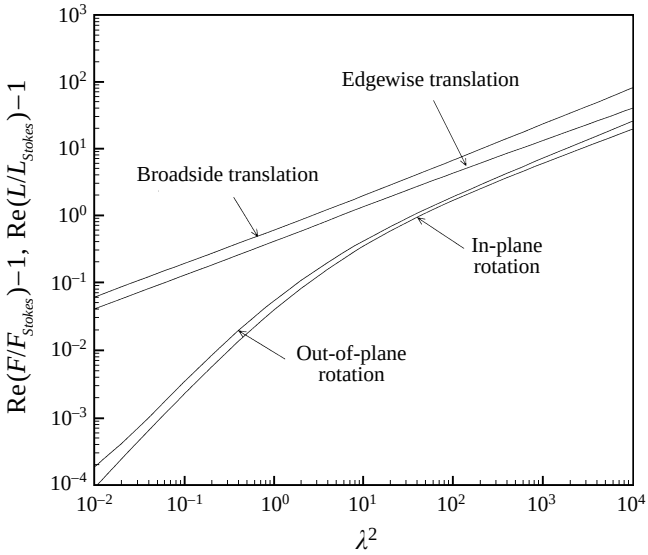

FIGURE 2. In-phase component of the non-dimensional hydrodynamic resistance (force F and torque L) calculated relative to the corresponding Stokes flow resistance (F_{Stokes} and L_{Stokes}) for each of the four motions shown in figure 1.

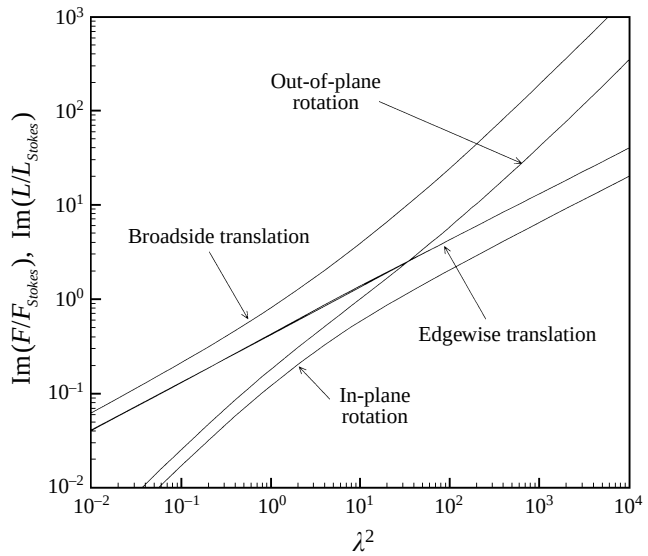

FIGURE 3. Out-of-phase component of the non-dimensional hydrodynamic resistance, normalized with respect to the Stokes resistance, for each of the four motions shown in figure 1.

In figure 2 we observe that the in-phase component of hydrodynamic resistance increases linearly with λ for all cases except for rotational oscillations at low frequencies, where it increases quadratically with λ. In contrast, the out-of-phase component of hydrodynamic resistance shown in figure 3 has a more complicated dependence on frequency. At low frequencies, a disk executing translational oscillations experiences a resistance that increases linearly with λ while a disk executing rotational oscillations experiences a resistance that increases quadratically with λ. At high frequencies, a

Motion	Force/Torque
(*a*) broadside translation	$F = -16\left[1 + \frac{8}{3\pi}e^{i\pi/4}\lambda + O(\lambda^2)\right]$
(*b*) edgewise translation	$F = -\frac{32}{3}\left[1 + \frac{16}{9\pi}e^{i\pi/4}\lambda + O(\lambda^2)\right]$
(*c*) in-plane rotation	$L = -\frac{32}{3}\left[1 + \frac{1}{5}i\lambda^2 + O(\lambda^3)\right]$
(*d*) out-of-plane rotation	$L = -\frac{32}{3}\left[1 + \frac{3}{10}i\lambda^2 + O(\lambda^3)\right]$

TABLE 1. Low-frequency asymptotic expressions for the force and torque on an oscillating disk. References: (*a*), (*b*) Williams (1966); (*c*) Kanwal (1970) – note that the sign of the low-frequency correction given by Kanwal is incorrect (see Appendix B); (*d*) Appendix B.

Motion	Force/Torque
(*a*) broadside translation	$F = -16\left[\frac{i\lambda^2}{6} + (1.32e^{i0.27\pi}\lambda)^* + O(1)\right]$
(*b*) edgewise translation	$F = -\frac{32}{3}\left[\frac{3\pi}{16}e^{i\pi/4}\lambda + O(1)\right]$
(*c*) in-plane rotation	$L = -\frac{32}{3}\left[\frac{3\pi}{32}e^{i\pi/4}\lambda + O(1)\right]$
(*d*) out-of-plane rotation	$L = -\frac{32}{3}\left[\frac{i\lambda^2}{30} + (0.43e^{i0.27\pi}\lambda)^* + O(1)\right]$

TABLE 2. High-frequency asymptotic expressions. * denotes values determined numerically from the results in figures 2 and 3.

disk that does not displace fluid as it oscillates experiences a resistance that increases linearly with λ, while a disk that displaces fluid as it oscillates experiences a resistance that increases quadratically with λ.

To discuss the numerical results in more detail we summarize in tables 1 and 2 the low- and high-frequency asymptotic estimates for the force and torque on an oscillating disk. All of the low-frequency asymptotic expressions, except the $O(\lambda^2)$ result for the out-of-plane rotary oscillation (see Appendix B for the detailed calculation), have appeared previously. The asymptotic expressions (*a*) and (*b*) in table 1 are specializations of a general formula for the dimensionless force $\mathrm{Re}(\boldsymbol{F}e^{it})$ on an arbitrarily shaped body executing low-frequency translational oscillations (Williams 1966):

$$\boldsymbol{F} = \boldsymbol{R}_{Stokes} \cdot \left[\boldsymbol{d} + \frac{\boldsymbol{R}_{Stokes} \cdot \boldsymbol{d}}{6\pi}\lambda e^{i\pi/4}\right] + O(\lambda^2), \tag{14}$$

where $\boldsymbol{R}_{Stokes}$ is the resistance tensor for Stokes flow ($\lambda = 0$) and $\boldsymbol{d}$ is a unit vector in the translation direction. Also included in table 2 and indicated by $*$ are numerically determined $O(\lambda)$ corrections to well-known potential flow results (Lamb 1932).

We have compared the asymptotic formulae with the detailed numerical results and the agreement is very good for low frequencies. Not surprisingly the error is largest at intermediate frequencies. For disk motions which do not displace fluid, the error can

be reduced by a composite formula which incorporates both low- and high-frequency asymptotic results, a topic we will consider further in § 5.

To gain some insight into why hydrodynamic resistance on an oscillating disk depends on frequency in the manner depicted in figures 2 and 3, we will identify the dominant contributions to the resistance in both the low- and high-frequency limits. At low frequencies the hydrodynamic resistance experienced by the disk is the Stokes flow resistance plus a small inertial correction. Since the disk acceleration is small ($\lambda^2 \ll 1$), inertial effects become significant only when we consider motion throughout a large fluid volume, which, from inspection of the unsteady Stokes equation, corresponds to motion on a length scale $O(a\lambda^{-1})$, a length scale much larger than the disk radius. On that length scale, a disk in translational oscillation appears approximately as an oscillating point force, which gives rise to an $O(\lambda)$ pressure-driven flow, thereby an $O(\lambda)$ correction to the dimensionless Stokes drag. In contrast, on the long $O(a\lambda^{-1})$ length scale, a disk in rotational oscillation appears as a point torque and a point source of stress. A point torque does not produce a pressure-driven flow but a point source of stress, or a stresslet, gives rise to a weaker, $O(\lambda^2)$ pressure-driven flow (e.g. Hocquart & Hinch 1983), thereby giving rise to an $O(\lambda^2)$ correction to the dimensionless Stokes torque.

For disk oscillations at high frequencies, $\lambda^2 \gg 1$, almost all of the fluid responds in an inviscid manner except for a thin boundary layer which is $O(a\lambda^{-1})$ in thickness adjacent to the disk surface. When the disk motion does not displace fluid, as for edgewise oscillations or in-plane rotary oscillations, the dominant hydrodynamic resistance is due to this Stokes boundary layer. As the oscillation frequency increases, the boundary layer dynamics corresponds closer and closer to that described by translational or rotational oscillations of an infinite plane (Stokes's first problem). When the disk motion involves displacement of surrounding fluid, as for broadside oscillations and out-of-plane rotations, the predominant hydrodynamic resistance at high frequency is the $O(\lambda^2)$ added mass term, which is $\pi/2$ out of phase with the disk motion, and hence does not contribute to energy dissipation. The $O(\lambda)$ correction to the resistance includes a $\pi/4$ out-of-phase viscous contribution from the Stokes boundary layer on the disk surface, as well as a contribution, due to the viscous boundary layer at the disk surface, which produces a modification of the pressure field from the inviscid pressure solution (Batchelor 1967). This correction is evident in figure 2, where the in-phase force and torque at high frequencies exhibit an $O(\lambda)$ dependence.

Lastly, we note that the hydrodynamic resistance on an oscillating oblate spheroid, based on viscous boundary layer theory, is singular in the limit of the oblate spheroid approaching a disk shape (Loewenberg 1993*a*) since in that limit the spheroid thickness becomes smaller than the boundary layer thickness; i.e. the boundary layer approximation breaks down. Our results for the hydrodynamic resistance on an oscillating disk of negligibly small thickness can then be used to yield a first-order estimate of the hydrodynamic resistance of a thin spheroid.

3.2. *Evolution of the fluid velocity fields*

There has been much recent interest in the structure of velocity fields associated with small-amplitude oscillatory motions. The adaptation of the boundary integral method from Stokes flow to unsteady Stokes flow has enabled researchers to study a regime of behaviour previously unamenable to detailed analysis, i.e. the regime in which fluid inertia and viscous stresses are equally important. Pozrikidis (1989*b*) calculated streamlines associated with translational oscillations of axisymmetric bodies while

Loewenberg (1993*a*, *b*, 1994*a*) calculated streamlines for cylinders in axisymmetric and transverse translational oscillations. Both authors have described the time evolution of the velocity field in terms of a cycle of nucleation, growth and disappearance of viscous eddies. This cycle is not found in either Stokes flows or potential flows and constitutes a unique and robust feature of oscillatory flows at intermediate frequencies. An analytical investigation of features of the eddy formation process is given by Smith (1995).

Not surprisingly, the cycle can also be observed in oscillatory flow of a disk in broadside oscillation or out-of-plane rotational oscillation. Figures 4 and 5 present calculated velocity fields for these two flows at dimensionless frequency $\lambda^2 = 1$. A perusal of these figures shows that the streamline patterns are very different from either the Stokes velocity fields, which correspond to low-frequency oscillations in which the fluid has sufficient time to viscously adjust to the disk motion and therefore always follows the motion of the disk, or the potential flow fields, which correspond to high-frequency oscillations in which fluid acceleration is the dominant effect and the fluid far from the disk always moves in the direction opposite that of the disk motion.

Before we go on to discuss particulars of figures 4 and 5, we note that the results are presented in the laboratory frame, where the particle is in motion and fluid far away is at rest, while previous studies have presented the calculated streamlines in the particle frame, where the particle is at rest and the fluid far away is oscillating. We have switched the reference frame because the viscous eddy evolution cycle takes on a much simpler form in the reference frame used here, from which it is straightforward to deduce the mechanism that gives rise to these eddies. Also, previous authors (Loewenberg 1993*a*, *b*; 1994*a*, *b*; Pozrikidis 1989*a*, *b*) have presented surface stress distributions at different frequencies. These distributions can also be calculated using the analytical solution developed in § 2, but will not be presented here as the results will differ only to a small degree from those calculated previously.

Now we begin a more detailed examination of the velocity fields. Figure 4 presents instantaneous streamline patterns over a half-cycle of broadside oscillation. The disk is aligned with the vertical r-axis and oscillates horizontally along the z-axis. Its velocity varies sinusoidally in time. Following our original assumption of small-amplitude oscillation, its centre of mass position is taken to be fixed at the origin. Since the flow is axisymmetric, we have calculated the values of streamlines analytically and they are labelled accordingly. Note the scales are adjusted to give the best illustration of the flow and hence are different at different times in the cycle. Figure 5 presents the analogous results for a disk in out-of-plane rotational oscillation. Note that the actual flow associated with a disk in out-of-plane rotational oscillation is three-dimensional. The velocity field is two-dimensional only in the normal plane, where the swirl component of the velocity is zero. Here we cannot obtain an analytical expression for the streamline values, but the velocity decays as $O(1/r^3)$ away from the disk.

Despite their apparent complexity, figures 4 and 5 look quite alike. Both seem to possess a two-part structure: an outer region far from the disk with a dipole-like velocity field pattern and an inner region near the disk which is composed of one or two eddies during most of the oscillation cycle.

We identify the inner region as a region of finite vorticity, in which, over an oscillation cycle, vorticities of opposite signs are alternately released. The vorticities diffuse outward and cancel each other, so that outside this region, the flow is essentially irrotational. In figures 4(*f*–*h*) or 5(*e*–*h*), one observes the cancellation as an older viscous eddy of one circulation is squeezed smaller and smaller by a growing eddy

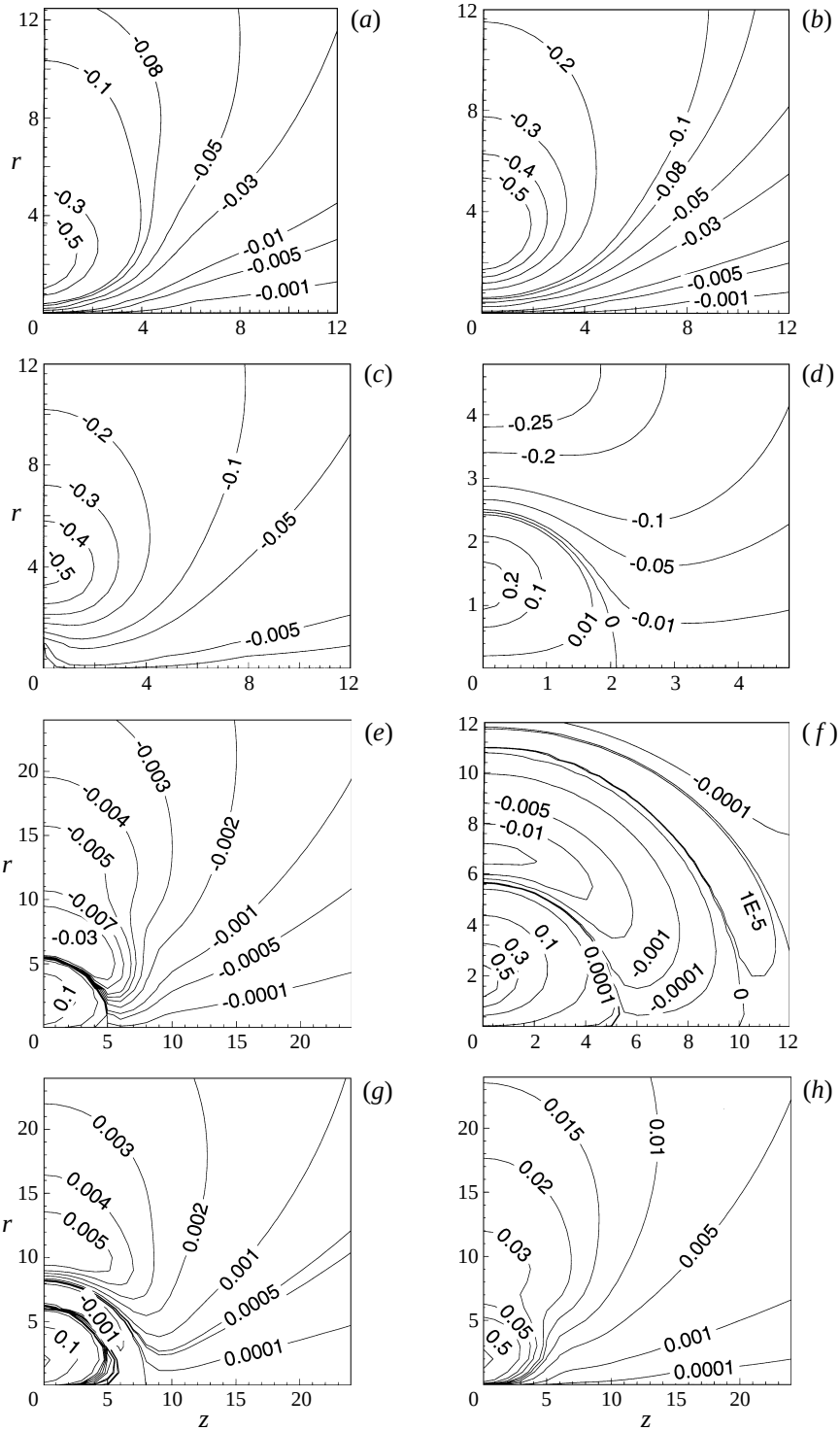

FIGURE 4. Velocity field for a disk in broadside oscillation for $\lambda^2 = 1$. Values of the stream function are indicated along the streamlines. Parts (*a–h*) correspond to $t = 0, 0.35\pi$, 0.5π, 0.65π, 0.84π, 0.85π, 0.86π and 0.90π.

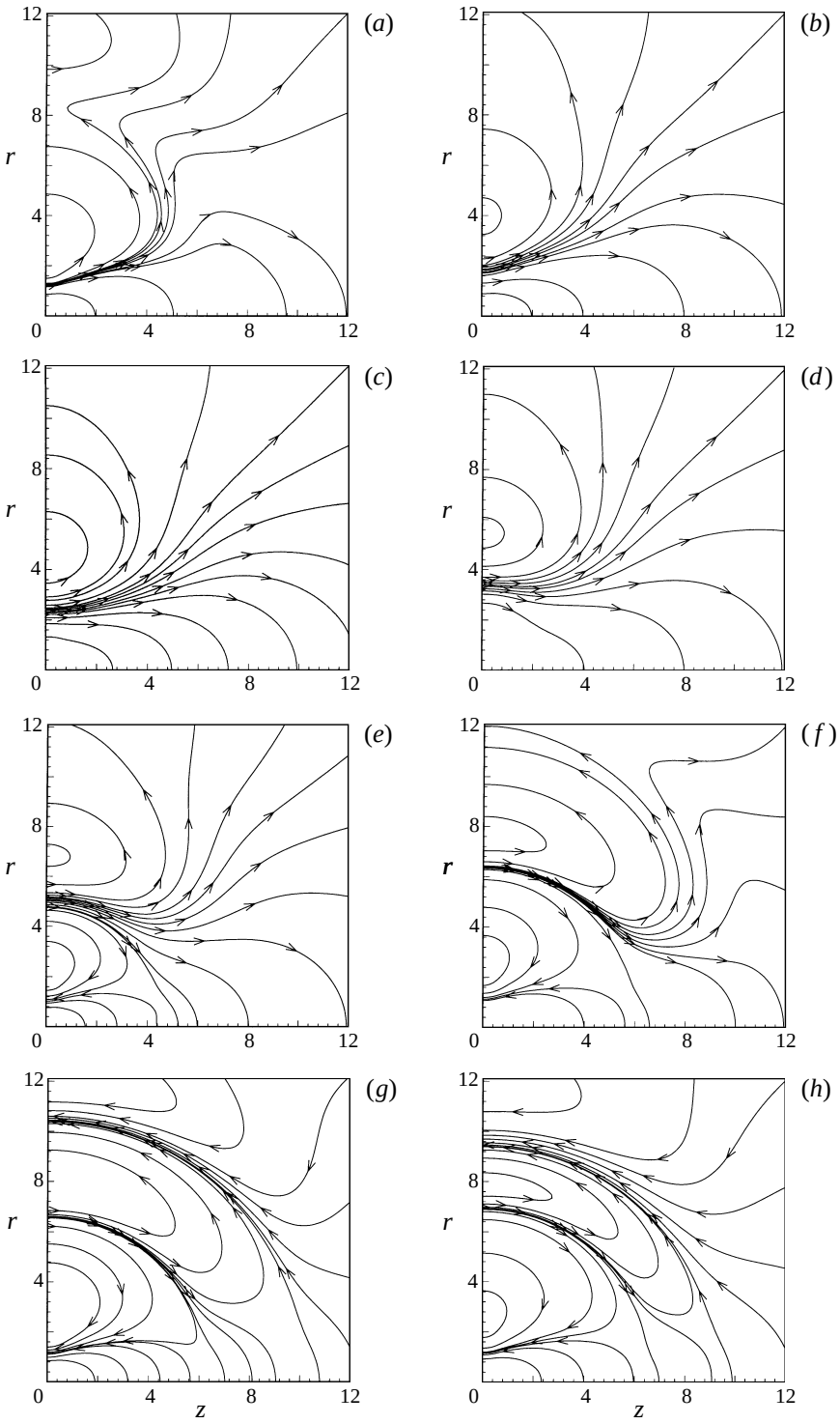

FIGURE 5. Velocity field for a disk in out-of-plane oscillation about the x-axis for $\lambda^2 = 1$. The flow is in the (y, z)-plane, $\theta = \pi/2$. Parts (a–h) correspond to $t = 0$, 0.35π, 0.5π, 0.65π, 0.85π, 0.94π, 0.95π and 0.96π.

of the opposite circulation. The process is much less obvious in the particle reference frame, where the viscous eddy appears to grow, detach from the disk, and then balloon out rapidly over a half-cycle.

We identify the outer region as the potential flow region. Here the disk motion appears as either an an oscillatory point force when the disk is in broadside translation, or as an oscillatory point source of stress when the disk is in out-of-plane rotational motion. (Note, though it is true that in the far field the rotating disk also appears to be a point torque, the point torque does not drive a flow in the far field.) Since the flow is not perfectly irrotational, the oscillation cycle of the point force or point source of stress seen by the far field does not correspond instantaneously to the oscillation cycle of the disk. When the disk reverses direction, the far-field flow does not immediately reverse so as to be moving in the direction opposite to that of the disk (as required by potential theory), but instead lags behind the oscillation cycle of the disk by some phase factor Φ. The phase factor Φ, which can be understood as the time required for the information that the disk has switched direction to diffuse through the finite-vorticity region and reach the potential flow region, increases linearly with the thickness of the boundary layer.

Alternatively, the phase lag can be understood by referring back to Stokes's (1851) work on an oscillating sphere or cylinder. By calculating the detailed velocity fields, Stokes showed that, for a sphere or a cylinder in high-frequency oscillation, the far field behaves as if the sphere or the cylinder has its radius increased by δ, where δ is the thickness of the vorticity boundary layer. Moreover, the effective centre of the sphere or cylinder lags behind the actual centre by δ (Batchelor 1967).

For broadside oscillation of a disk, we have compared values of the phase lag Φ deduced from the calculated streamlines with values computed by taking the hydrodynamic resistance experienced by an oscillatory sphere as the value of the point force singularity driving the far-field flow. The point force solution is

$$\boldsymbol{w}_{\mathrm{pt-force}} = -\mathrm{i}F\boldsymbol{U}\cdot\left[\frac{1}{4\pi\lambda^2}\left(\frac{\boldsymbol{I}}{r^3}-\frac{3\boldsymbol{rr}}{r^5}\right)-(\boldsymbol{I}\nabla^2-\nabla\nabla)\frac{\mathrm{e}^{-\lambda r/\sqrt{2}}\mathrm{e}^{-\mathrm{i}\lambda r/\sqrt{2}}}{4\pi\lambda^2 r}\right] \tag{15}$$

where r is distance from origin. Since the second term in brackets decays exponentially the far-field velocity field is determined by the first term, which corresponds to the potential flow solution due to an oscillating point force $-F(\lambda)\boldsymbol{U}$. Recalling that the non-dimensional velocity field is given by $\boldsymbol{u} = \mathrm{Re}(\boldsymbol{w}\mathrm{e}^{\mathrm{i}t})$ and writing the complex force function as $F(\lambda) = -|F|\mathrm{e}^{\mathrm{i}\Phi}$ (note: $0 \leqslant \Phi < \pi/2$), we see the far-field flow has the structure

$$\boldsymbol{u}_{\mathrm{pt-force}} = -\mathrm{Re}(\mathrm{e}^{\mathrm{i}(t-(\pi/2-\Phi))})\frac{|F|\boldsymbol{U}}{4\pi\lambda^2}\cdot\left(\frac{\boldsymbol{I}}{r^3}-\frac{3\boldsymbol{rr}}{r^5}\right) \quad \text{as } |\boldsymbol{r}|\to\infty, \tag{16}$$

where we have written the equation explicitly displaying a negative sign to be consistent with the far-field potential flow which moves, along $z = 0$, in a direction opposite to the disk. Therefore, there is a phase lag $\pi/2-\Phi$ between the imposed disk motion and the far-field motion. Here Φ can be evaluated approximately using the results for a spherical particle

$$\Phi_{sphere} = \tan^{-1}\{\lambda(1+\sqrt{2}\lambda/9)/(\sqrt{2}+\lambda)\}. \tag{17}$$

The above analytic formula gives good agreement with values of phase lag deduced from numerical calculations. Also, the agreement improves slightly if we use asymp-

totic expressions in tables 1 and 2 for the hydrodynamic resistance experienced by the disk instead of the sphere.

We have calculated streamlines for different oscillation frequencies and observe essentially the same cycle of streamline evolution. As expected, the thickness of the finite-vorticity region, and hence the far-field phase lag Φ, decrease with increasing frequency. The other two modes of disk motion illustrated in figure 1 do not displace fluid and for these modes the structure of the associated velocity field can be deduced easily.

Finally, we note that our analysis of disk motion has been based on the assumption that flow separation does not occur. In general, for oscillatory flow past a solid body, flow separation occurs when the oscillation amplitude is comparable to the radius of curvature of the disk edge (Batchelor 1967 p. 353). Thus, if we consider our results to be an approximate model of a real disk-shaped particle with rounded edges, we expect the results reported here to be valid for sufficiently small-amplitude oscillations.

4. Oscillatory motions of a nearly spherical particle

4.1. *Preliminary remarks*

We now turn our attention from oscillatory motions of a disk to oscillatory motions of a nearly spherical particle. The well-studied Stokes flow limit ($\lambda = 0$) is discussed by Happel & Brenner (1965). Approximate analytic expressions for the hydrodynamic resistance on the oscillating near sphere will be derived via the reciprocal theorem and compared with available numerical results. These expressions represent generalizations of the well known applications of the reciprocal theorem in Stokes flow problems.

Our work is motivated by recent results concerning the translation of symmetric bodies. Lawrence & Weinbaum (1988) obtained an exact expression for the hydrodynamic resistance experienced by a spheroid in axisymmetric translational oscillation. These authors noted that, provided the spheroid aspect ratio is between 0.1 and 10, the force $\mathrm{Re}(\mu|\boldsymbol{U}|a\boldsymbol{F}\,\mathrm{e}^{\mathrm{i}\omega t})$ on a spheroid with minor axis radius a and translating with velocity $\boldsymbol{U}\cos\omega t$ is well approximated by the following composite formula for the low- and high-frequency asymptotic expansions:

$$\boldsymbol{F} \approx \left(\boldsymbol{R}_{Stokes} + \mathrm{e}^{\mathrm{i}\pi/4}\lambda\boldsymbol{B}_\infty + \mathrm{i}\lambda^2\boldsymbol{M}_a + \frac{\mathrm{e}^{\mathrm{i}\pi/4}\lambda}{1+\mathrm{e}^{\mathrm{i}\pi/4}\lambda}(\boldsymbol{R}_1 - \boldsymbol{B}_\infty)\right)\cdot\boldsymbol{U}, \tag{18}$$

where $\lambda^2 = \omega a^2/\nu$. In (18), $\boldsymbol{R}_{Stokes}$ is the Stokes resistance tensor for the spheroid, $\boldsymbol{B}_\infty$ is the Basset tensor, $\boldsymbol{R}_1$ is the first-order correction to the Stokes resistance tensor at low-frequency, and $\boldsymbol{M}_a$ is the added mass tensor. The second and third terms on the right-hand side represent the high-frequency asymptotic limit. The last term represents a correction to the expansion so that the formula tends to the correct low-frequency asymptotic expansion. For a sphere, $\boldsymbol{B}_\infty = \boldsymbol{R}_1$, so that the last term vanishes, and the force has a quadratic dependence on λ. Lawrence & Weinbaum's observation, i.e. equation (18), has been confirmed and extended by numerical studies (Pozrikidis 1989*a*, *b*, Loewenberg 1993*a*, *b*, 1994*a*, *b*), which demonstrate that (18) works for transversely oscillating spheroids, as well as finite cylinders undergoing translational oscillations, provided the aspect ratio remains moderate. In these cases, the difference between $\boldsymbol{B}_\infty$ and $\boldsymbol{R}_1$ has been found to be small regardless of the detailed particle geometry or type of translational oscillation. Section 4.2 provides some theoretical justification for this observation by considering translational motions of a slightly non-spherical particle.

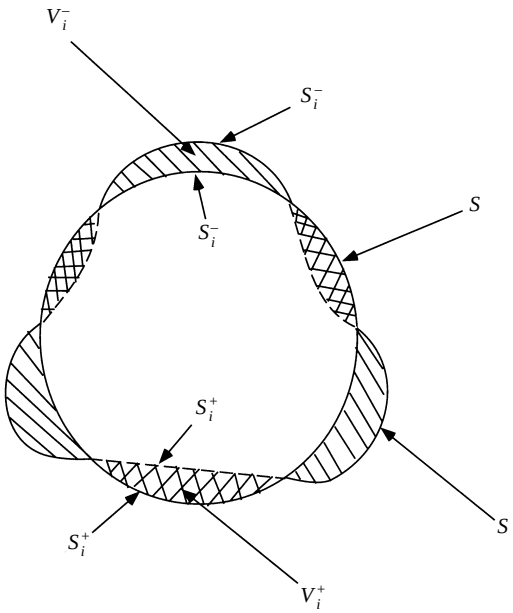

FIGURE 6. A sphere inscribed in a nearly spherical body.

The analysis in § 4.2 can be easily generalized to arbitrary oscillatory motions, provided that the unsteady Stokes flow approximation holds. In that case, we expect a particle translating with velocity $\mathrm{Re}(\boldsymbol{U}_o e^{it})$ and rotating with angular velocity $\mathrm{Re}(\boldsymbol{\Omega}_o e^{it})$ to experience a hydrodynamic force $\mathrm{Re}(\boldsymbol{F} e^{it})$ and a hydrodynamic torque $\mathrm{Re}(\boldsymbol{L} e^{it})$ where $\boldsymbol{F}$ and $\boldsymbol{L}$ are linearly related to $\boldsymbol{U}_o$ and $\boldsymbol{\Omega}_o$:

$$\begin{pmatrix} \boldsymbol{F} \\ \boldsymbol{L} \end{pmatrix} = \begin{pmatrix} \boldsymbol{A} & \boldsymbol{B} \\ \boldsymbol{C} & \boldsymbol{D} \end{pmatrix} \cdot \begin{pmatrix} \boldsymbol{U}_o \\ \boldsymbol{\Omega}_o \end{pmatrix}. \tag{19}$$

The second-rank tensors $\boldsymbol{A}$, $\boldsymbol{B}$, $\boldsymbol{C}$ and $\boldsymbol{D}$ depend on the dimensionless oscillation frequency λ^2 and the detailed particle geometry. It follows from the linearity of the unsteady Stokes equations that $\boldsymbol{A}$ and $\boldsymbol{D}$ are symmetric tensors and $\boldsymbol{B} = \boldsymbol{C}^{\mathrm{T}}$. Section 4.2 ascertains the form of $\boldsymbol{A}$; § 4.3 then determines the hydrodynamic torque resistance tensor $\boldsymbol{D}$ and the coupling tensor $\boldsymbol{C}$. From results for hydrodynamic resistance on nearly spherical bodies in Stokes flow (Rallison 1978), we expect, and shall indeed find that, in the limit of small deviations from a sphere, the first-order effects of shape variation depend only on the second spherical harmonic component, i.e. for the hydrodynamic resistance, all nearly spherical bodies can be approximated to first-order in their deviations from a sphere by equivalent ellipsoids. One consequence of this observation is that the coupling between rotation and translation is a small effect and does not show up as a first-order correction.

Finally, § 4.4 contains approximate expressions for the hydrodynamic resistance on a nearly spherical body in arbitrary time-dependent motion, which are derived via standard Laplace transform ideas from formulae obtained in §§ 4.2–4.3. Throughout § 4 we shall take the characteristic length scale to be the radius of an equal-volume sphere, the characteristic time scale to be the inverse of the oscillation frequency and the characteristic velocity scale to be the maximum oscillation velocity.

4.2. *Translational oscillatory motions of a nearly spherical particle*

In this subsection, we will relate, via the reciprocal theorem, the hydrodynamic resistance experienced by an oscillating nearly spherical particle to the hydrodynamic resistance experienced by an equal-volume sphere oscillating at the same frequency. Consider a nearly spherical body in translational oscillation with velocity $\boldsymbol{U}_o e^{it}$. In spherical coordinates, the surface of the nearly spherical body is $r = 1 + \epsilon f(\theta, \phi)$ with $\epsilon \ll 1$, where r has already been non-dimensionalized by the radius of an equal-volume sphere. At $O(\epsilon)$, this choice of length scale implies that

$$\int_{\hat{S}} f \, dS = 0 \tag{20}$$

where $\hat{S}$ is the surface of the equivalent-volume sphere. We will also fix the origin at the centre of mass of the nearly spherical body. This choice of coordinate system implies that

$$\int_{\hat{S}} \boldsymbol{n} f \, dS = \boldsymbol{0} \tag{21}$$

and leads to a particularly simple form of the hydrodynamic resistance tensor for the nearly spherical body.

The problem is illustrated in figure 6. $\hat{S}$ denotes the surface of the sphere and S denotes the surface of the nearly spherical particle. As conventional, the unit normal points into the fluid. It is convenient to choose the sphere centre to coincide with the centre of mass of the nearly spherical particle. Since they have the same volume, this choice of relative placement means parts of the nearly spherical particle extend beyond the sphere. We have shaded these volumes in stripes and labelled them V_i^-, $i = 1 \ldots N$, where N is the total number of bumps the nearly spherical particle has over the surface of an equal-volume sphere. Similarly, we label the parts of the sphere surface that bound volumes V_i^- as $\hat{S}_i^-$ and label the parts of the nearly spherical particle surface that bound V_i^- as S_i^-. In the same spirit, parts of the sphere which extend beyond the nearly spherical particle are labelled as V_i^+, bounded by surfaces $\hat{S}_i^+$ and S_i^+.

To write out the governing equations for the sphere and the nearly spherical particle, we let $\mathrm{Re}(\boldsymbol{u}e^{it})$ and $\mathrm{Re}(pe^{it})$ denote the non-dimensional velocity and pressure fields due to oscillation of the nearly spherical body (although this notation is slightly different than that used in § 2, the presentation here is self-contained so that there should be no confusion). Also, let $\mathrm{Re}(\hat{\boldsymbol{u}}e^{it})$ and $\mathrm{Re}(\hat{p}e^{it})$ denote the non-dimensional velocity and pressure fields due to the oscillation of a sphere of equal volume. We then have

$$i\lambda^2 \boldsymbol{u} = \nabla \cdot \boldsymbol{T}, \quad \nabla \cdot \boldsymbol{u} = 0 \quad \text{with } \boldsymbol{u}|_S = \boldsymbol{U}_o \tag{22a}$$

$$i\lambda^2 \hat{\boldsymbol{u}} = \nabla \cdot \hat{\boldsymbol{T}}, \quad \nabla \cdot \hat{\boldsymbol{u}} = 0 \quad \text{with } \hat{\boldsymbol{u}}|_{\hat{S}} = \hat{\boldsymbol{U}}_o, \tag{22b}$$

where $\boldsymbol{T}$ and $\hat{\boldsymbol{T}}$ are stress tensors. The fluid at infinity is quiescent for both flows.

Applying the reciprocal theorem, equations (22*a*) and (22*b*) may be rearranged to give

$$0 = \nabla \cdot (\boldsymbol{T} \cdot \hat{\boldsymbol{u}}) - \nabla \cdot (\hat{\boldsymbol{T}} \cdot \boldsymbol{u}). \tag{23}$$

Now let V_1 denote the volume of fluid outside the sphere and let V_2 denote the volume of fluid outside the nearly spherical particle. Clearly, since the particles have equal volumes, $V_1 = V_2 = V_2 + V^- - V^+$ where $V^- = \sum_{i=1}^{N} V_i^-$ and $V^+ = \sum_{i=1}^{N} V_i^+$,

so that integrating over the fluid volume outside the sphere, (23) becomes

$$0 = \int_{V_2+(V^- - V^+)} \nabla \cdot (\boldsymbol{T} \cdot \hat{\boldsymbol{u}}) \mathrm{d}V - \int_{V_1} \nabla \cdot (\hat{\boldsymbol{T}} \cdot \boldsymbol{u}) \mathrm{d}V. \tag{24}$$

We then break the first integral into three parts and apply the divergence theorem to the volume integrals over V_1 and V_2. Keeping in mind that $\boldsymbol{n}$ points into the fluid, we obtain

$$0 = -\int_S \boldsymbol{n} \cdot \boldsymbol{T} \cdot \hat{\boldsymbol{u}} \mathrm{d}S + \int_{V^-} \nabla \cdot (\boldsymbol{T} \cdot \hat{\boldsymbol{u}}) \mathrm{d}V - \int_{V^+} \nabla \cdot (\boldsymbol{T} \cdot \hat{\boldsymbol{u}}) \mathrm{d}V + \int_{\hat{S}} \boldsymbol{n} \cdot \hat{\boldsymbol{T}} \cdot \boldsymbol{u} \mathrm{d}S \tag{25}$$

where $\int_{V^-}$ and $\int_{V^+}$ are taken to represent the sum of the volume integrals over each of the volumes V_{i}^+ or V_{i}^-. As usual in Stokes flow calculations, the velocity and stress distributions for both flows decay sufficiently rapidly for the surface integrals at infinity to vanish. Considering the second and third terms together, we first note that the integrand can be rewritten as $\mathrm{i}\lambda^2 \boldsymbol{u} \cdot \hat{\boldsymbol{u}}$ by using the fact that within each V_i^- the particle velocity is that of a solid body translation $\boldsymbol{U}_o$ while within each V_i^+ the sphere velocity is that of a solid body translation $\hat{\boldsymbol{U}}_o$. We then have

$$\int_{V^-} \nabla \cdot (\boldsymbol{T} \cdot \hat{\boldsymbol{u}}) \mathrm{d}V - \int_{V^+} \nabla \cdot (\boldsymbol{T} \cdot \hat{\boldsymbol{u}}) \mathrm{d}V = \mathrm{i}\lambda^2 \left(\int_{V^-} \hat{\boldsymbol{u}} \mathrm{d}V \cdot \boldsymbol{U}_o - \int_{V^+} \boldsymbol{u} \mathrm{d}V \cdot \hat{\boldsymbol{U}}_o \right). \tag{26}$$

We next make use of the fact that the particle is nearly spherical and approximate the volume integrals as surface integrals over regions on the equal-volume sphere which bound each of the volumes in V^+ or V^-, whereupon we arrive at

$$\int_{V^-} \nabla \cdot (\boldsymbol{T} \cdot \hat{\boldsymbol{u}}) \mathrm{d}V - \int_{V^+} \nabla \cdot (\boldsymbol{T} \cdot \hat{\boldsymbol{u}}) \mathrm{d}V = \mathrm{i}\lambda^2 \boldsymbol{U}_o \cdot \hat{\boldsymbol{U}}_o \left(\sum_{i=1}^{N} \int_{\hat{S}_i^-} \epsilon f \mathrm{d}S + \sum_{i=1}^{N} \int_{\hat{S}_i^+} \epsilon f \mathrm{d}S \right). \tag{27}$$

Note that $f < 0$ for V^+, therefore the (defined as positive only) volume element is approximated as $-\epsilon f \mathrm{d}S$. The quantity in the parentheses above is simply the surface integral of f over an unit sphere, which is zero by (21). Therefore the reciprocal relation between the hydrodynamic resistance on a nearly spherical particle in translational oscillation and that on an equal-volume sphere in translational oscillation has the same form as the Stokes flow result:

$$\int_S \boldsymbol{n} \cdot \boldsymbol{T} \cdot \hat{\boldsymbol{u}} \mathrm{d}S = \int_{\hat{S}} \boldsymbol{n} \cdot \hat{\boldsymbol{T}} \cdot \boldsymbol{u} \mathrm{d}S. \tag{28}$$

To evaluate (28), we begin by noting that, on the nearly spherical surface S, the velocity field associated with the equal-volume sphere in translational oscillation is a uniform solid body translation over S_i^+, as points on S_i^+ are inside the sphere. On the other hand, the velocity field due to the equal-volume sphere over S_i^- is $\hat{\boldsymbol{u}}_o + \epsilon f \partial \hat{\boldsymbol{u}} / \partial r|_{r=1} + O(\epsilon^2)$ as these regions lie outside the sphere.

The velocity field due to the nearly spherical body evaluated on the spherical surface is slightly more complicated. First we write the velocity field as a regular perturbation expansion in ϵ:

$$\boldsymbol{u} = \boldsymbol{u}^{(0)} + \epsilon \boldsymbol{u}^{(1)} + O(\epsilon^2). \tag{29}$$

The zeroth-order term corresponds to the velocity field due to a sphere translating with velocity $\boldsymbol{U}_o$ in unsteady Stokes flow. A regular perturbation expansion about the boundary condition on the particle surface then yields $\boldsymbol{u}^{(1)}|_{r=1} = -\epsilon f \partial \boldsymbol{u}^{(0)} / \partial r|_{r=1}$. Putting these results together, the velocity field evaluated on the surface $\hat{S}$ of the

equivalent-volume sphere is

$$\boldsymbol{u}|_{\hat{S}} = \boldsymbol{U}_o \text{ over } \hat{S}_i^-, \tag{30a}$$

$$\boldsymbol{u}|_{\hat{S}} = \boldsymbol{U}_o - \epsilon f \frac{\partial \boldsymbol{u}^{(0)}}{\partial r}\bigg|_{r=1} + O(\epsilon^2) \text{ over } \hat{S}_i^+. \tag{30b}$$

After substituting these expressions into (28), we use the fact that corrections to the velocity field are $O(\epsilon)$ and approximate surface integrals over the nearly spherical particle surface as those over a unit sphere, an approximation that only introduces $O(\epsilon^2)$ errors. Keeping in mind that

$$\left(\int_S \boldsymbol{n}\cdot\boldsymbol{T}\,\mathrm{d}S\right)\cdot\hat{\boldsymbol{U}}_o = \boldsymbol{F}\cdot\hat{\boldsymbol{U}}_o \quad \text{and} \quad \left(\int_{\hat{S}} \boldsymbol{n}\cdot\hat{\boldsymbol{T}}\,\mathrm{d}S\right)\cdot\boldsymbol{U}_o = \hat{\boldsymbol{F}}\cdot\boldsymbol{U}_o, \tag{31}$$

where $\mathrm{Re}(\boldsymbol{F}\mathrm{e}^{\mathrm{i}t})$ and $\mathrm{Re}(\hat{\boldsymbol{F}}\mathrm{e}^{\mathrm{i}t})$ are the non-dimensional hydrodynamic resistance experienced, respectively, by the near sphere and the equal-volume sphere, we rewrite (28) as

$$\boldsymbol{F}\cdot\hat{\boldsymbol{U}}_o = \hat{\boldsymbol{F}}\cdot\boldsymbol{U}_o - \sum_{i=1}^{N}\int_{\hat{S}_i^-}\boldsymbol{n}\cdot\boldsymbol{T}^{(0)}\cdot\left(\epsilon f\frac{\partial\hat{\boldsymbol{u}}}{\partial r}\bigg|_{r=1}\right)\mathrm{d}S - \sum_{i=1}^{N}\int_{\hat{S}_i^+}\boldsymbol{n}\cdot\hat{\boldsymbol{T}}\cdot\left(\epsilon f\frac{\partial\boldsymbol{u}^{(0)}}{\partial r}\bigg|_{r=1}\right)\mathrm{d}S. \tag{32}$$

Note that we have replaced $\boldsymbol{T}$ and $\boldsymbol{u}$ in the $O(\epsilon)$ surface integrals by $\boldsymbol{T}^{(0)}$ and $\boldsymbol{u}^{(0)}$. Finally, we use well-known results for a sphere in translational oscillation to evaluate the surface stress and the radial velocity gradient. If the oscillation velocity is $\boldsymbol{U}^*$ we have

$$\boldsymbol{n}\cdot\boldsymbol{T}^*|_{\hat{S}} = -\tfrac{1}{2}\left[3(\mathrm{e}^{\mathrm{i}\pi/4}\lambda+1)\boldsymbol{I} + \mathrm{i}\lambda^2\boldsymbol{nn}\right]\cdot\boldsymbol{U}^*, \tag{33a}$$

$$\frac{\partial\boldsymbol{u}^*}{\partial r}\bigg|_{\hat{S}} = -\tfrac{3}{2}(\mathrm{e}^{\mathrm{i}\pi/4}\lambda+1)(\boldsymbol{I}-\boldsymbol{nn})\cdot\boldsymbol{U}^*. \tag{33b}$$

In (32), the relations (33) are used for both $\hat{\boldsymbol{T}}$, $\partial\hat{\boldsymbol{u}}/\partial r$ as well as $\boldsymbol{T}^{(0)}$, $\partial\boldsymbol{u}^{(0)}/\partial r$. Also recall that the hydrodynamic resistance $\hat{\boldsymbol{F}}$ experienced by an oscillating sphere is given by

$$\hat{\boldsymbol{F}} = -6\pi\left(1+\mathrm{e}^{\mathrm{i}\pi/4}\lambda+\frac{\mathrm{i}\lambda^2}{9}\right)\hat{\boldsymbol{U}}_o. \tag{34}$$

Using expressions (33) and (34) as well as the fact that $\hat{\boldsymbol{U}}_o$ is an arbitrary vector, the hydrodynamic resistance on a nearly spherical particle in translational oscillation is given by

$$\boldsymbol{F} = -\left[6\pi\left(1+\mathrm{e}^{\mathrm{i}\pi/4}\lambda+\frac{\mathrm{i}\lambda^2}{9}\right)\boldsymbol{I} - \frac{9(\mathrm{e}^{\mathrm{i}\pi/4}\lambda+1)^2\epsilon}{4}\int_S f\boldsymbol{nn}\mathrm{d}S + O(\epsilon^2)\right]\cdot\boldsymbol{U}_o. \tag{35}$$

Note that the first term is the resistance on the equal-volume sphere while the second term is a correction due to shape deviations. Both terms are quadratic in λ, which implies that the difference in the $O(\lambda)$ coefficient for the force at low and high frequencies is at most an $O(\epsilon^2)$ effect, i.e. $\boldsymbol{R}_1 - \boldsymbol{B}_\infty = O(\epsilon^2)$, and so helps to explain why Lawrence & Weinbaum's (1988) composite formula (18) has been found to work well for translational oscillations of a variety of body shapes, not simply spheroids.

For an oblate particle in axisymmetric translation, equation (35) agrees to $O(\epsilon)$ with Lawrence & Weinbaum's (1986) formula. Note that since this flow is axisymmetric, Lawrence & Weinbaum were able to obtain an $O(\epsilon^2)$ formula by solving for the detailed velocity and pressure fields with a stream function formulation. For a prolate

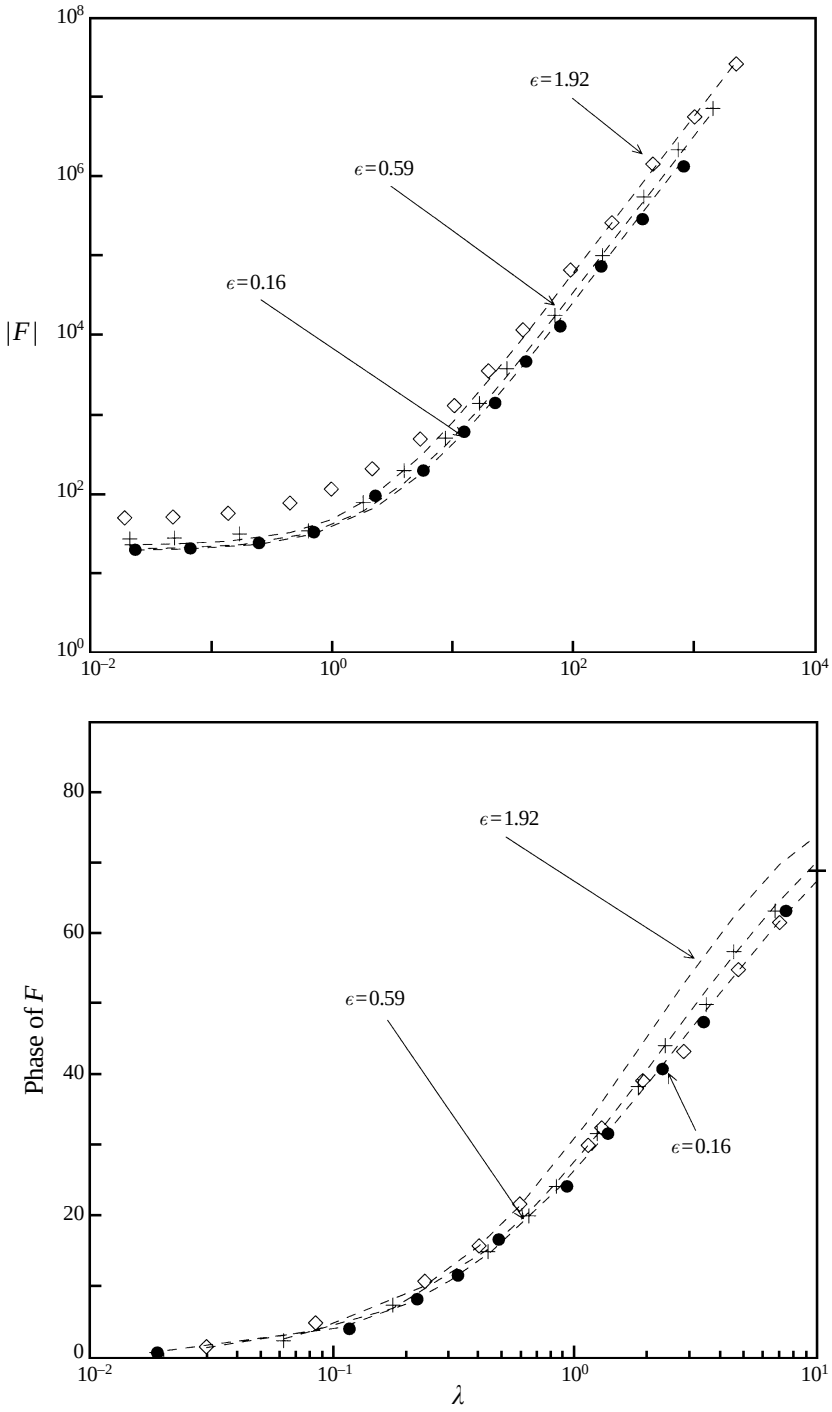

FIGURE 7. Magnitude and phase of the hydrodynamic resistance on a prolate spheroid in transverse oscillation. Dashed curves denote predictions from the asymptotic formula (35). Symbols denote Pozrikidis's (1989*a*, figure 4) numerical results: $\epsilon = 0.16$ corresponds to the major axis radius to minor axis radius ratio $a/b = 1.25$ used by Pozrikidis and is represented by dark circles; $\epsilon = 0.59$ corresponds to $a/b = 2.0$ and is represented by plus signs; $\epsilon = 1.92$ corresponds to $a/b = 5.0$ and is represented by diamonds.

spheroid aligned with the y-axis in translational oscillation and an oblate spheroid in transverse translational oscillation, (35) reduces to Kim & Karrila's (1991) result for Stokes flow ($\lambda = 0$) as well as simplifying to Lamb's (1932) result for inviscid flow ($\lambda \to \infty$).

We have also compared the analytical result (35) with numerically calculated values of the hydrodynamic resistance experienced by a prolate spheroid in transverse oscillation (Pozrikidis 1989*a*, figure 4). Figure 7 presents the comparison for the magnitude and phase of the hydrodynamic resistance where the dashed curves are the analytical predictions and the symbols are numerically calculated results (the variables a and b that Pozrikidis uses to denote the radii of the major and minor axes of the ellipsoid are related to our ϵ by $\epsilon = (a/b)^{2/3} - 1$.) For nearly spherical shapes, i.e. for small ϵ, the analytical results are in good agreement with the numerical results for all λ.

4.3. *Arbitrary oscillatory motions of a nearly spherical particle*

We now consider a nearly spherical particle in purely rotational oscillation about an axis through its centre of mass. The details of the analysis follow § 4.2 closely. Again we start with equations (22), but now use the boundary conditions $\boldsymbol{u}|_S = \boldsymbol{\Omega}_o \wedge \boldsymbol{r}$ and $\hat{\boldsymbol{u}}|_{\hat{S}} = \hat{\boldsymbol{\Omega}}_o \wedge \boldsymbol{r}$. Following the steps outlined earlier, we combine equations (22*a*) and (22*b*) then integrate the resultant equation over the fluid volume outside the sphere. But now, due to the fact that

$$\boldsymbol{r}|_S = \boldsymbol{r}|_{\hat{S}} + \epsilon f \boldsymbol{r}|_{\hat{S}} + O(\epsilon^2), \tag{36}$$

the integrals over V^- and V^+ no longer vanish. Some manipulation shows

$$\int_{V^-} \nabla \cdot (\boldsymbol{T} \cdot \hat{\boldsymbol{u}}) \mathrm{d}V - \int_{V^+} \nabla \cdot (\boldsymbol{T} \cdot \hat{\boldsymbol{u}}) \mathrm{d}V = \mathrm{i}\lambda^2 \boldsymbol{\Omega}_o \hat{\boldsymbol{\Omega}}_o : \int_{\hat{S}} \epsilon f \boldsymbol{nn} \mathrm{d}S \tag{37}$$

so the reciprocal relation has the form

$$\int_S \boldsymbol{n} \cdot \boldsymbol{T} \cdot \hat{\boldsymbol{u}} \mathrm{d}S = \int_{\hat{S}} \boldsymbol{n} \cdot \hat{\boldsymbol{T}} \cdot \boldsymbol{u} \mathrm{d}S + \mathrm{i}\lambda^2 \boldsymbol{\Omega}_o \hat{\boldsymbol{\Omega}}_o : \int_{\hat{S}} \epsilon f \boldsymbol{nn} \mathrm{d}S. \tag{38}$$

Next we approximate $\boldsymbol{u}|_{\hat{S}}$ and $\hat{\boldsymbol{u}}|_S$ as

$$\hat{\boldsymbol{u}}|_S = \hat{\boldsymbol{\Omega}}_o \wedge \boldsymbol{r}|_{r=1} + \epsilon f \frac{\partial \hat{\boldsymbol{u}}}{\partial \boldsymbol{r}} \text{ over } S_i^-, \tag{39a}$$

$$= \hat{\boldsymbol{\Omega}}_o \wedge \boldsymbol{r}|_{r=1} \text{ over } S_i^+, \tag{39b}$$

$$\boldsymbol{u}|_{\hat{S}} = \boldsymbol{\Omega}_o \wedge \boldsymbol{r}|_{r=1} \text{ over } \hat{S}_i^-, \tag{39c}$$

$$= \boldsymbol{\Omega}_o \wedge \boldsymbol{r}|_{r=1} - \epsilon f \frac{\partial \boldsymbol{u}^{(0)}}{\partial \boldsymbol{r}} \text{ over } \hat{S}_i^+, \tag{39d}$$

where again $\boldsymbol{u}^{(0)}$ is the zeroth-order velocity field for $\boldsymbol{u}$ and corresponds to the velocity field due to a sphere in rotational oscillation with angular velocity $\boldsymbol{\Omega}_o$. Substituting (39) into (38), we obtain an expression for the hydrodynamic torque on the particle in terms of a sum of surface integrals. We then approximate $\boldsymbol{T}$ in the $O(\epsilon)$ surface integrals by $\boldsymbol{T}^{(0)}$ and use the following relations, derived for a sphere rotating with angular velocity $\mathrm{Re}(\boldsymbol{\Omega}^* \mathrm{e}^{\mathrm{i}t})$:

$$\boldsymbol{n} \cdot \boldsymbol{T}^*|_{\hat{S}} = -\left(\frac{\mathrm{i}\lambda^2}{\mathrm{e}^{\mathrm{i}\pi/4}\lambda + 1} + 3 \right) \boldsymbol{\Omega}^* \wedge \boldsymbol{n}, \tag{40a}$$

$$\left.\frac{\partial \boldsymbol{u}^*}{\partial r}\right|_{\hat{S}} = -\left(\frac{\mathrm{i}\lambda^2}{\mathrm{e}^{\mathrm{i}\pi/4}\lambda + 1} + 2\right)\boldsymbol{\Omega}^* \wedge \boldsymbol{n}. \tag{40b}$$

Substituting the above expressions for $\boldsymbol{T}, \hat{\boldsymbol{T}}^{(0)}, \partial\hat{\boldsymbol{u}}/\partial r$ and $\partial\boldsymbol{u}^{(0)}/\partial r$ in (38) and using the formula for hydrodynamic torque $\hat{\boldsymbol{L}}$ on a sphere in oscillatory rotation

$$\hat{\boldsymbol{L}} = -\frac{8\pi}{3}\left(\frac{\mathrm{i}\lambda^2}{\mathrm{e}^{\mathrm{i}\pi/4}\lambda + 1} + 3\right)\hat{\boldsymbol{\Omega}}_o, \tag{41}$$

we find the hydrodynamic torque $\mathrm{Re}(\boldsymbol{L}\mathrm{e}^{\mathrm{i}t})$ on a nearly spherical particle

$$\boldsymbol{L}(\lambda) = \left[-\frac{8\pi}{3}\left(\frac{\mathrm{i}\lambda^2}{\mathrm{e}^{\mathrm{i}\pi/4}\lambda + 1} + 3\right)\boldsymbol{I} + \epsilon\left[\left(\frac{\mathrm{i}\lambda^2}{\mathrm{e}^{\mathrm{i}\pi/4}\lambda + 1} + 3\right)^2 - \mathrm{i}\lambda^2\right]\int_{\hat{S}} f\boldsymbol{nn}\,\mathrm{d}S\right]\cdot\boldsymbol{\Omega}_o \tag{42}$$

which defines $\boldsymbol{D}(\lambda)$. The integral involving the shape function f is the same as the integral that appears in equation (35) and so, in fact, no extra work is needed to construct $\boldsymbol{D}$ once $\boldsymbol{A}$ is determined.

We note that in the high-frequency limit equation (42) does not have an $O(\lambda^2)$ contribution, which must exist if the rotating object displaces surrounding fluid. Thus, we conclude that the added mass resistance experienced by a rotating near sphere is at most an $O(\epsilon^2)$ term. Potential flow solutions (Lamb 1932) for rotation of an ellipsoid confirm this result and show that indeed the added mass resistance is $O(\epsilon^2\lambda^2)$. Therefore, at the next order the approximate result (42) must have a correction that is $O(\epsilon^2\lambda^2)$. For a body that displaces fluid as it rotates, it is thus necessary to require $\epsilon\lambda \ll 1$ (in addition to $\epsilon \ll 1$) for (42) to be used. Equation (42) has been compared with recent numerical calculations of the hydrodynamic torque experienced by a prolate or an oblate spheroid in axisymmetric rotational oscillation (Tekasakul, Tompson & Loyalka 1998) for the cases $\epsilon = 0.2$ and $\epsilon = 0.1$. The numerical results and the analytic expression show the expected agreement.

Finally, we discuss the coupling of translational and rotational oscillations. We shall find that, provided the axis of rotation goes through the centre of mass, the coupling between translational and rotational oscillations is an $O(\epsilon^2)$ effect. This is consistent with results derived in the Stokes flow limit.

Again, we follow the reciprocal theorem approach. Suppose the nearly spherical particle is translating with velocity $\mathrm{Re}(\boldsymbol{U}_o\mathrm{e}^{\mathrm{i}t})$. To consider the hydrodynamic torque exerted on the nearly spherical particle due to its translational oscillation, we compare the flow problem with that of an equivalent-volume sphere in oscillatory rotation with angular velocity $\mathrm{Re}(\hat{\boldsymbol{\Omega}}_o\mathrm{e}^{\mathrm{i}t})$. The steps are similar to those used above with the difference being that the integrals over V^- and V^+ in (25) now take the form

$$\int_{V^-}\nabla\cdot(\boldsymbol{T}\cdot\hat{\boldsymbol{u}})\mathrm{d}V + \int_{V^+}\nabla\cdot(\boldsymbol{T}\cdot\hat{\boldsymbol{u}})\mathrm{d}V = \mathrm{i}\lambda^2\boldsymbol{\Omega}_o \wedge \int_{\hat{S}}\boldsymbol{n}\epsilon f\,\mathrm{d}S\cdot\boldsymbol{U}_o, \tag{43}$$

while corrections to $O(1)$ approximate velocities on the sphere and particle surfaces also yield an integral of the form above. Taken together, the final form for the induced hydrodynamic torque $\mathrm{Re}(\boldsymbol{L}\mathrm{e}^{\mathrm{i}t})$ is

$$\boldsymbol{L} = -\frac{9\epsilon}{2}\left(1 + \mathrm{e}^{\mathrm{i}\pi/4}\lambda + \frac{\mathrm{i}\lambda^2}{9}\right)\int_{\hat{S}}\boldsymbol{n}f\,\mathrm{d}S \wedge \boldsymbol{U}_o. \tag{44}$$

Recall that fixing the origin at the centre of mass requires $\int_{\hat{S}} f\boldsymbol{n}\mathrm{d}s = \boldsymbol{0}$, so therefore the $O(\epsilon)$ coupling contribution vanishes. Note that (44) should not be taken as an estimate of the coupling experienced by a nearly spherical particle which is rotated

about an axis that does not go through its centre of mass, since in obtaining (44) we have compared the velocity field due to a nearly spherical particle to that of a sphere rotated about its centre of mass. The proper comparison would start with a sphere which is rotated about an equally off-centre axis.

4.4. *Time-dependent motion of a nearly spherical body*

Time-dependent motion of a particle can be studied in a standard fashion by taking a Laplace transform with respect to time of (2) and setting $\lambda^2 = 1$, which corresponds to scaling time with the viscous diffusion scale a^2/ν (e.g. Lawrence & Weinbaum 1986). We shall denote the Laplace transform variable as s. The solution of the transformed equation is now equivalent to (3) with $\mathrm{i} \to s$. Therefore, given analytical expressions for $\boldsymbol{F}(\lambda)$ and $\boldsymbol{L}(\lambda)$, for the force and torque experienced by a body in oscillatory motion (§§ 4.2–4.4), it is only necessary to perform an inverse Laplace transform to formally obtain the time-dependent force and torque on a particle.

Before presenting the explicit formulae, we recall that for the particle motion problems considered here the unsteady Stokes equation is approximate with an $O(\mathscr{R})$ error (Lovalenti & Brady 1993). Hence, for $\mathscr{R} \ll 1$ the Laplace transform solution is actually an incorrect approximation to the Navier-Stokes equations for $|s| < \mathscr{R}$, which implies that the long-time behavior of the hydrodynamic resistance will deviate from that predicted according to an unsteady Stokes flow analysis. A thorough discussion of this difficult topic is given by Lovalenti & Brady (1993).

Here we confine ourselves to obtaining the time-dependent hydrodynamic resistance for a near sphere based on the unsteady Stokes flow approximation. The particle is assumed to translate with velocity $\boldsymbol{U}(t)$ and the detailed shape is given by $r = 1 + \epsilon f(\theta, \phi)$. The force then follows by taking the inverse Laplace transform of the appropriately modified ($\lambda = 1, \mathrm{i} \to s$) equation (35):

$$-\frac{\boldsymbol{F}(t)}{6\pi} = (\boldsymbol{I} - \epsilon \boldsymbol{H}_1) \cdot \boldsymbol{U} + (\boldsymbol{I} - 2\epsilon \boldsymbol{H}_1) \cdot \int_0^t \frac{\mathrm{d}\boldsymbol{U}}{\mathrm{d}\tau} \frac{\mathrm{d}\tau}{(\pi(t-\tau))^{1/2}} + [\tfrac{1}{9}\boldsymbol{I} - \epsilon \boldsymbol{H}_1] \cdot \frac{\mathrm{d}\boldsymbol{U}}{\mathrm{d}t} \tag{45}$$

where $\boldsymbol{H}_1$ is given by

$$\boldsymbol{H}_1 = \frac{3}{8\pi} \int_{\hat{S}} f \boldsymbol{nn} \, \mathrm{d}S. \tag{46}$$

The time-dependencies in (45) correspond to the instantaneous Stokes force, the Basset history term and the added mass and (45) explicitly accounts for small, arbitrary changes from a spherical shape. The additional memory term first noted by Lawrence & Weinbaum (1986) for nearly spherical, spheroidal particles is an $O(\epsilon^2)$ effect.

For a nearly spherical body experiencing a time-dependent rotation, $\boldsymbol{\Omega}(t)$, we may also use these Laplace transform ideas. However, the $O(\epsilon)$ formula (42) for the torque on a near sphere fails to capture the added mass resistance at high frequencies (an $O(\epsilon^2)$ effect), and therefore we can only obtain the time-dependent torque for axisymmetric rotations. In this case, we find that the time-dependent torque is (the inverse Laplace transform utilizes results in Oberhettinger & Badii 1973)

$$-\frac{\boldsymbol{L}(t)}{8\pi} = (\boldsymbol{I} - \epsilon \boldsymbol{H}_1) \cdot \boldsymbol{\Omega}(t) + \frac{1}{3} \int_0^t \frac{\mathrm{d}\boldsymbol{\Omega}}{\mathrm{d}\tau} \left[\frac{1}{(\pi(t-\tau))^{1/2}} - \mathrm{e}^{t-\tau} \mathrm{erfc}((t-\tau)^{1/2}) \right] \mathrm{d}\tau$$
$$-\tfrac{1}{3}\epsilon \boldsymbol{H}_1 \cdot \int_0^t \frac{\mathrm{d}\boldsymbol{\Omega}}{\mathrm{d}\tau} \left[\frac{4}{(\pi(t-\tau))^{1/2}} - (5 - 2(t-\tau)) \mathrm{e}^{t-\tau} \mathrm{erfc}((t-\tau)^{1/2}) - 2 \left(\frac{t-\tau}{\pi} \right)^{1/2} \right] \mathrm{d}\tau. \tag{47}$$

At $O(\epsilon)$ the torque $\boldsymbol{L}(t)$ on a nearly spherical object has *additional* memory terms as compared to the case of a rotating sphere (Feuillebois & Lasek 1978; see also Gatignol 1983). These additional terms, in particular the $O(\epsilon/(t-\tau)^{1/2})$ contribution, represent a slightly stronger emphasis on recent history than for the case of a rotating sphere. Finally we note that the form of the time-dependent force and torque have the general form predicted by Gavze (1990).

5. Composite expansion formulae for hydrodynamic resistance on a disk in unsteady Stokes flow

With the understanding we have developed for non-spherical shapes, we now return briefly to the circular disk shapes discussed in §§ 2–3. Lawrence & Weinbaum demonstrated that the composite formula (18) worked well for aspect ratios 0.1 to 10. Here we test (18) for the limiting case of a circular disk. Our results indicate that (18), and a similar formula for rotation, work tolerably well for, respectively, edgewise oscillations and in-plane rotational oscillations, but not for broadside oscillations and out-of-plane rotational oscillations.

In particular, for a translating disk the force is given by $\mathrm{Re}(\mu U a \boldsymbol{F} \mathrm{e}^{\mathrm{i}\omega t})$. Following Lawrence & Weinbaum (1988), $\boldsymbol{F}$ for edgewise oscillation has the form

$$\boldsymbol{F} = -\frac{32}{3}\left[1 + \frac{3\pi}{16}\mathrm{e}^{\mathrm{i}\pi/4}\lambda + \left(\frac{16}{9\pi} - \frac{3\pi}{16}\right)\frac{\mathrm{e}^{\mathrm{i}\pi/4}\lambda}{1+\mathrm{e}^{\mathrm{i}\pi/4}\lambda}\right]\boldsymbol{U}. \tag{48}$$

Note that the coefficient of the third term is very small ($16/9\pi - 3\pi/16 \approx -0.023$) and so for all practical purposes the first two terms of either the low- or high-frequency expansions provide an excellent approximation for all frequencies. This result is similar to a conclusion reached by Davis (1993*a*).

We next turn to in-plane rotational oscillations. Motivated by Lawrence & Weinbaum's success combining the low- and high-frequency behaviour into a composite formula for all frequencies, we constructed an approximate formula for the torque using as a guide our results for a nearly spherical body in rotational oscillations (see equation (42) and rearrange the $O(\epsilon)$ coefficients). Thus, we propose that the torque $\mathrm{Re}(\mu\Omega a^3 \boldsymbol{L}\mathrm{e}^{\mathrm{i}wt})$ is approximately

$$\boldsymbol{L} = -\frac{32}{3}\left[1 + \frac{3\pi}{32}\frac{\mathrm{i}\lambda^2}{\mathrm{e}^{\mathrm{i}\pi/4}\lambda + 1} + \left(\frac{1}{5} - \frac{3\pi}{32}\right)\frac{\mathrm{i}\lambda^2}{(\mathrm{e}^{\mathrm{i}\pi/4}\lambda + 1)^2}\right]\boldsymbol{\Omega}, \tag{49}$$

where the second term in brackets is the high-frequency limit (table 2) and the third term is chosen to provide the correct low-frequency limit. Again, note that the coefficient for the third term ($\frac{1}{5} - 3\pi/32 \approx -0.095$) is small. Comparing with numerically calculated values, (48) and (49) each have maximum errors of 6% for $10^{-3} < \lambda^2 < 10^5$, being least accurate for $\lambda \approx 10$.

On the other hand, we attempted similar composite expansion schemes for broadside oscillations and out-of-plane rotational oscillations. Using numerically estimated values of $O(\lambda)$ corrections at high frequencies, these expansions were found to be less successful and to have maximum errors of about 35%.

Since the forms of the composite formulae are motivated by results for nearly spherical bodies, there is no reason *a priori* to expect them to be accurate for circular disks. Lawrence & Weinbaum (1988) stated that the formula (18) for translation is restricted to modest aspect ratios, while Loewenberg's numerical studies (1993*b*) of finite cylinders in arbitrary translational oscillations indicate that (18) is less accurate

for cylinders of extreme aspect ratios. However, we observed that the formula works well for edgewise translation of a circular disk.

6. Conclusions

In this paper we have presented a study of translational and rotational oscillatory motions of disk-shaped and nearly spherical particles. Exact solutions for disk shapes allowed the investigation of forces and torques as a function of frequency as well as the evolution of the flow. Although we did not obtain the flow field for the arbitrarily shaped particles, it is possible, using the reciprocal theorem, to obtain the frequency dependence of the resistance tensors.

Several extensions of this work seem possible. Motivated by the analogy of the circular disk shape to shapes representative of valves, gears and levers designed into microelectromechanical devices, it may be worthwhile to consider changes in the hydrodynamic resistance for finite Knudsen numbers as well as accounting for the influence of nearby planar boundaries. Both effects may be studied using the analytical approach outlined in §2. In addition, steady streaming flows (Batchelor 1967) typically accompany oscillatory boundary motions. These secondary flows arise owing to nonlinear terms and may be studied by using the solutions to the unsteady Stokes equations given in this paper.

We thank M. Loewenberg for several helpful conversations regarding oscillatory Stokes flow, J. M. Rallison for insightful suggestions regarding the resistance of nearly spherical particles and the referees for their thoughtful comments. Also, we thank the NSF for support of this research through grant CTS-94-23228 (HAS) and an NSF graduate research fellowship (W.Z.).

Appendix A. Summary of the analytical solutions for translational and rotational oscillations of a disk

In this Appendix we present a brief summary of the analysis of broadside and edgewise translational oscillations and in-plane rotational oscillations of a circular disk. These solutions complement the solution for out-of-plane oscillations which was given in § 2.2 and the solution methodology has the same form. The notation established in § 2.2 is used consistently with $\boldsymbol{u} = \mathrm{Re}(\boldsymbol{w}\mathrm{e}^{\mathrm{i}t})$ and $p = \mathrm{Re}(Q\mathrm{e}^{\mathrm{i}t})$ denoting, respectively, the nondimensional velocity and pressure fields. The solution for edgewise translational oscillations, developed using dual integral equation ideas, but presented with a different form of solution, was given by Davis (1993*a*).

We begin by deducing the angular dependence of the velocity and pressure fields from the on-disk boundary conditions. In particular, broadside translational oscillations and in-plane rotational oscillations give rise to axisymmetric flows. Moreover, an in-plane rotational oscillation gives rise to a purely azimuthal (swirl) velocity field and a dynamic pressure field that vanishes everywhere. On the other hand, for edgewise oscillations along the x-axis, the no-slip boundary condition on the disk, $r < 1, z = 0$ (expressed in cylindrical coordinates), is $\boldsymbol{w} = (\cos\theta, \sin\theta, 0)$. Table 3 summarizes the boundary conditions applied at $z = 0$ for each mode of motion and table 4 summarizes the form of solution sought for the velocity and pressure fields.

To construct explicit solutions we take Hankel transforms of the momentum equations. For edgewise oscillation, we again decouple the momentum equations by working in terms of $v_r + v_\theta, v_r - v_\theta, v_z$ and q while for the other problems it is sufficient

Motion	$\forall r$	$r<1$	$r>1$
(*a*) broadside translation	$v_r=0$	$v_z=1$	$q=0$
(*b*) edgewise translation	$v_z=0$	$v_r=1,\ v_\theta=-1$	$\dfrac{\partial v_r}{\partial z}=\dfrac{\partial v_\theta}{\partial z}=0$
(*c*) in-plane rotation	NA	$v_\theta=1$	$\dfrac{\partial v_\theta}{\partial z}=0$
(*d*) out-of-plane rotation	$v_r=v_\theta=0$	$v_z=r\sin\theta$	$q=0$

TABLE 3. Boundary conditions for oscillatory motions of a disk.

Motion	w_r	w_θ	w_z	Q
(*a*) broadside translation	$v_r(r,z)$	0	$v_z(r,z)$	$q(r,z)$
(*b*) edgewise translation	$v_r(r,z)\cos\theta$	$v_\theta(r,z)\sin\theta$	$v_z(r,z)\cos\theta$	$q(r,z)\cos\theta$
(*c*) in-plane rotation	0	$v_\theta(r,z)$	0	0
(*d*) out-of-plane rotation	$v_r(r,z)\sin\theta$	$v_\theta(r,z)\cos\theta$	$v_z(r,z)\sin\theta$	$q(r,z)\sin\theta$

TABLE 4. Functional form of the velocity and pressure fields.

to work with the original variables. Following the steps outlined in § 2, the solutions for the different particle motions may be shown to have the form

(i) broadside oscillation:

$$v_r(r,z)=\int_0^\infty kB(k)\left(\mathrm{e}^{-kz}-\mathrm{e}^{-\ell z}\right)J_1(kr)\,\mathrm{d}k, \tag{A 1a}$$

$$v_z(r,z)=\int_0^\infty kB(k)\left(\mathrm{e}^{-kz}-\frac{k}{\ell}\mathrm{e}^{-\ell z}\right)J_0(kr)\,\mathrm{d}k, \tag{A 1b}$$

$$q(r,z)=\mathrm{i}\lambda^2\int_0^\infty B(k)\mathrm{e}^{-kz}J_0(kr)\,\mathrm{d}k; \tag{A 1c}$$

(ii) edgewise oscillation:

$$v_r(r,z)=\frac{1}{2}\int_0^\infty k\left[\left(D(k)-\frac{2\ell}{k}C(k)\right)\mathrm{e}^{-\ell z}+C(k)\mathrm{e}^{-kz}\right]J_2(kr)\,\mathrm{d}k$$
$$+\frac{1}{2}\int_0^\infty k\left[D(k)\mathrm{e}^{-\ell z}-C(k)\mathrm{e}^{-kz}\right]J_0(kr)\,\mathrm{d}k, \tag{A 2a}$$

$$v_\theta(r,z)=\frac{1}{2}\int_0^\infty k\left[\left(D(k)-\frac{2\ell}{k}C(k)\right)\mathrm{e}^{-\ell z}+C(k)\mathrm{e}^{-kz}\right]J_2(kr)\,\mathrm{d}k$$
$$-\frac{1}{2}\int_0^\infty k\left[D(k)\mathrm{e}^{-\ell z}-C(k)\mathrm{e}^{-kz}\right]J_0(kr)\,\mathrm{d}k, \tag{A 2b}$$

$$v_z(r,z)=\int_0^\infty kC(k)(\mathrm{e}^{-kz}-\mathrm{e}^{-\ell z})J_1(kr)\,\mathrm{d}k, \tag{A 2c}$$

$$q(r,z)=\mathrm{i}\lambda^2\int_0^\infty C(k)\mathrm{e}^{-kz}J_1(kr)\,\mathrm{d}k; \tag{A 2d}$$

(iii) in-plane rotational oscillation:

$$v_\theta(r,z)=\int_0^\infty kE(k)J_1(kr)\mathrm{e}^{-\ell z}\,\mathrm{d}k, \tag{A 3a}$$

$$v_r(r,z) = v_z(r,z) = q(r,z) = 0. \tag{A 3b}$$

Again, $\ell = ((k^2 + \mathrm{i}\lambda^2)^{1/2})$ and the positive square root is taken.

The functions $B(k), C(k), D(k)$, and $E(k)$ satisfy dual integral conditions derived from the on- and off-disk boundary conditions at $z = 0$:

(i) broadside oscillation:

$$\int_0^\infty kB(k)\left(1 - \frac{k}{\ell}\right) J_0(kr)\,\mathrm{d}k = 1, \quad r < 1, \tag{A 4}$$

$$\int_0^\infty B(k) J_0(kr)\,\mathrm{d}k = 0, \quad r > 1; \tag{A 5}$$

(ii) edgewise oscillation:

$$\int_0^\infty [kD(k) + (k - 2\ell)C(k)]\, J_2(kr)\,\mathrm{d}k = 0, \quad r < 1, \tag{A 6a}$$

$$\int_0^\infty k\,[D(k) - C(k)]\, J_0(kr)\,\mathrm{d}k = 2, \quad r < 1, \tag{A 6b}$$

$$\int_0^\infty \left[\ell^2 C(k) - k\ell D(k)\right] J_2(kr)\,\mathrm{d}k = 0, \quad r > 1, \tag{A 6c}$$

$$\int_0^\infty \left[k^2 C(k) - k\ell D(k)\right] J_0(kr)\,\mathrm{d}k = 0, \quad r > 1; \tag{A 6d}$$

(iii) in-plane oscillatory rotation:

$$\int_0^\infty kE(k) J_1(kr)\,\mathrm{d}k = r, \quad r < 1, \tag{A 7a}$$

$$\int_0^\infty k\ell E(k) J_1(kr)\,\mathrm{d}k = 0, \quad r > 1. \tag{A 7b}$$

Using Tranter's method (Tranter 1966), we represent the unknown functions as a Bessel function series so that the integral equations corresponding to the off-disk boundary conditions ($r > 1, z = 0$) are automatically satisfied. Hence, we take

$$B(k) = k^{1-\beta} \sum_{m=0}^{\infty} b_m J_{2m+\beta}(k), \tag{A 8a}$$

$$E(k) = \frac{k^{-\beta}}{\ell} \sum_{m=0}^{\infty} e_m J_{1+2m+\beta}(k). \tag{A 8b}$$

For edgewise oscillations, instead of solving for $C(k)$ and $D(k)$ directly, it is convenient to solve for related functions $F(k)$ and $G(k)$ where

$$C(k) = -\frac{\mathrm{i}k}{2\lambda^2}\,[F(k) - G(k)]\,, \tag{A 9a}$$

$$D(k) = \frac{\mathrm{i}}{2\lambda^2\ell}\left[\ell^2 G(k) - k^2 F(k)\right], \tag{A 9b}$$

and $F(k)$ and $G(k)$ have the form

$$F(k) = k^{-\alpha} \sum_{m=0}^{\infty} f_m J_{2+2m+\alpha}(k), \tag{A 10a}$$

$$G(k) = k^{-\beta} \sum_{m=0}^{\infty} g_m J_{2m+\beta}(k). \tag{A 10b}$$

We set $\beta = \alpha = 1/2$ to capture the stress singularity at the disk edge.

Finally, constants $\{b_m\}, \{e_m\}, \{f_m\}$ and $\{g_m\}$ in the Bessel function series are determined by solving a linear system of equations derived from the integral equations corresponding to the on-disk boundary conditions ($r < 1, z = 0$). The linear systems are given below. After the coefficients $\{b_m\}, \{e_m\}, \{f_m\}, \{g_m\}$ are determined, the detailed fluid velocity fields about the circular disk are known:

(i) broadside oscillation:

$$\sum_{m=0}^{\infty} b_m \int_0^{\infty} k^{2-2\beta} \left(1 - \frac{k}{\ell}\right) J_{2m+\beta}(k) J_{2n+\beta}(k)\, \mathrm{d}k = \frac{\delta_{0n}}{2^{\beta}\Gamma(1+\beta)}, \quad n = 0, 1, \cdots, \tag{A 11}$$

(ii) edgewise oscillation:

$$\sum_{m=0}^{\infty} g_m R_{mn} + f_m S_{mn} = \frac{2\ \delta_{0n}}{2^{\alpha}\Gamma(\alpha+2)}, \quad n = 0, 1, \cdots, \tag{A 12a}$$

$$\sum_{m=0}^{\infty} g_m \hat{R}_{mn} + f_m \hat{S}_{mn} = 0, \quad n = 0, 1, \cdots, \tag{A 12b}$$

with $R_{mn}, S_{mn}, \hat{R}_{mn}$, and $\hat{S}_{mn}$ given by

$$R_{mn} = \int_0^{\infty} k^{1-2\alpha} \left(1 - \frac{k}{\ell}\right) J_{2n+\alpha}(k) J_{2m+\alpha}(k)\, \mathrm{d}k, \tag{A 13a}$$

$$S_{mn} = \frac{\mathrm{i}}{\lambda^2} \int_0^{\infty} k^{2-(\alpha+\beta)} \left(1 - \frac{k}{\ell}\right) J_{2n+\alpha}(k) J_{2+2m+\beta}(k)\, \mathrm{d}k, \tag{A 13b}$$

$$\hat{R}_{mn} = \frac{\mathrm{i}}{\lambda^2} \int_0^{\infty} k^{2-(\alpha+\beta)} \left(1 - \frac{k}{\ell}\right) J_{2+2n+\beta}(k) J_{2m+\alpha}(k)\, \mathrm{d}k, \tag{A 13c}$$

$$\hat{S}_{mn} = \int_0^{\infty} k^{1-2\beta} \left(1 - \frac{k}{\ell}\right) J_{2+2n+\beta}(k) J_{2+2m+\beta}(k)\, \mathrm{d}k; \tag{A 13d}$$

(iii) in-plane rotational oscillation:

$$\sum_{m=0}^{\infty} e_m \int_0^{\infty} \frac{k^{1-2\beta}}{\ell} J_{1+2m+\beta}(k) J_{1+2n+\beta}(k)\, \mathrm{d}k = \frac{\delta_{0n}}{2^{\beta}\Gamma(2+\beta)}, \quad n = 0, 1, \cdots. \tag{A 14}$$

The non-dimensional hydrodynamic force and torque exerted by the fluid on the disk are calculated, respectively, by integrating the surface stress distribution and its first moment, over both sides of the disk. Again, by choosing $\beta = 1/2$ only the coefficient of the first term in the Bessel series (A 8) or (A 10) is required to obtain the hydrodynamic resistance. We find

(i) broadside oscillation:

$$\boldsymbol{F} = -4\lambda^2 (2\pi)^{1/2} \mathrm{i} b_0 \boldsymbol{e}_z; \tag{A 15}$$

(ii) edgewise oscillation:

$$\boldsymbol{F} = -2(2\pi)^{1/2} \mathrm{i} g_0 \boldsymbol{e}_x; \tag{A 16}$$

(iii) in-plane rotation:

$$\boldsymbol{L} = -\frac{4(2\pi)^{1/2}}{3} \mathrm{i} e_0 \boldsymbol{e}_z. \tag{A 17}$$

The calculated hydrodynamic force and torque on the oscillating disk are presented in § 3.1.

Appendix B. Torque for low-frequency rotational oscillations

Asymptotic expressions are available for the hydrodynamic resistance for the low-frequency broadside and edgewise oscillatory translations of a thin disk in unsteady Stokes flow and for in-plane low-frequency rotations (Kanwal 1970; Williams 1966). To the best of our knowledge, the corresponding expression for the torque has not been given for low-frequency out-of-plane rotations so we derive the result in this Appendix.

Consider a body oscillating with angular velocity $\boldsymbol{\Omega}\cos\omega t$ in a viscous fluid. We use the same non-dimensionalization as described in the text and so wish to solve (3) subject to the boundary conditions $\boldsymbol{w}|_{S_p} = \boldsymbol{\Omega}\wedge\boldsymbol{r}$, and at infinity $(|\boldsymbol{w}|, Q) \to 0$. We shall use the reciprocal theorem and so introduce the corresponding Stokes flow velocity and pressure fields, $\hat{\boldsymbol{w}}$ and $\hat{Q}$, which satisfy

$$\boldsymbol{0} = -\nabla\hat{Q} + \nabla^2\hat{w} = \nabla\cdot\hat{\boldsymbol{T}} \quad \text{and} \quad \nabla\cdot\hat{w} = 0, \tag{B 1}$$

where $\hat{\boldsymbol{T}}$ is the usual stress tensor, and $\hat{\boldsymbol{w}}$ and $\hat{Q}$ satisfy boundary conditions $\hat{\boldsymbol{w}}|_{S_p} = \boldsymbol{\Omega}\wedge\boldsymbol{r}$ and $(\hat{\boldsymbol{w}}, \hat{Q}) \to 0$ as $|\boldsymbol{r}| \to \infty$. Then, developing the reciprocal theorem for equations (3) and (B 1) leads to

$$\mathrm{i}\lambda^2\boldsymbol{w}\cdot\hat{\boldsymbol{w}} = \nabla\cdot(\boldsymbol{T}\cdot\hat{\boldsymbol{w}}) - \nabla\cdot(\hat{\boldsymbol{T}}\cdot\boldsymbol{w}). \tag{B 2}$$

Integrating over the fluid volume, applying the divergence theorem, and using the boundary conditions on the particle surface, we obtain

$$\boldsymbol{L}\cdot\boldsymbol{\Omega} = \hat{\boldsymbol{L}}\cdot\boldsymbol{\Omega} - \mathrm{i}\lambda^2\int_V \boldsymbol{w}\cdot\hat{\boldsymbol{w}}\,\mathrm{d}V, \tag{B 3}$$

where $\boldsymbol{L}$ denotes the torque experienced by the body undergoing oscillatory rotation, $\hat{\boldsymbol{L}}$ denotes the torque experienced by the rotating body in Stokes flow, and V is the fluid volume surrounding the particle. Now, for $\lambda^2 \ll 1$, a representation for $\boldsymbol{w}$ can be constructed using the method of matched asymptotic expansions. The 'inner expansion' in λ, with $\hat{\boldsymbol{w}}$ being the zeroth-order solution, is

$$\boldsymbol{w} = \hat{\boldsymbol{w}} + \lambda\boldsymbol{w}^{(1)} + \lambda^2\boldsymbol{w}^{(2)} + \cdots \tag{B 4}$$

and an outer solution is needed on length scales $|\boldsymbol{r}| > O(1/\lambda)$. The field $\boldsymbol{w}^{(1)}$ corresponds to a correction to the Stokes velocity field produced by a far-field flow where the local acceleration ($\mathrm{i}\lambda^2\boldsymbol{w}$) is important. In general, a rotating non-spherical body at low Reynolds numbers is characterized by combination of a rotlet and stresslet in the far field (Hocquart & Hinch 1983). This far-field flow has $\boldsymbol{w} = O(\lambda^2)$ which corresponds to an $O(\lambda^2)$ correction to the inner velocity field. Hence $\boldsymbol{w}^{(1)} = \boldsymbol{0}$ everywhere for a body experiencing low-frequency oscillatory rotations and the leading-order correction is $O(\lambda^2)$.

We may then substitute $\hat{w}$ for $\boldsymbol{w}$ in the integral (B 3) to arrive at a formula for the torque on a body in low-frequency oscillatory rotation:

$$\boldsymbol{L}\cdot\boldsymbol{\Omega} = \hat{\boldsymbol{L}}\cdot\boldsymbol{\Omega} - \mathrm{i}\lambda^2\int_V \hat{\boldsymbol{w}}\cdot\hat{\boldsymbol{w}}\,\mathrm{d}V + O(\lambda^3). \tag{B 5}$$

For out-of-plane rotations of a disk, the corresponding Stokes velocity fields are given

by Tanzosh & Stone (1996). In particular, owing to symmetry it is only necessary to consider $z > 0$ for which

$$\hat{w}_r = \frac{2\cos\theta}{\pi}\int_0^\infty \left(k^{-1}\sin k - \cos k\right) z\mathrm{e}^{-kz}\left[J_2(kr) - J_0(kr)\right]\mathrm{d}k, \tag{B 6a}$$

$$\hat{w}_\theta = \frac{2\sin\theta}{\pi}\int_0^\infty \left(k^{-1}\sin k - \cos k\right) z\mathrm{e}^{-kz}\left[J_2(kr) + J_0(kr)\right]\mathrm{d}k, \tag{B 6b}$$

$$\hat{w}_z = \frac{4\cos\theta}{\pi}\int_0^\infty k^{-1}\left(k^{-1}\sin k - \cos k\right)(1+zk)\mathrm{e}^{-zk}J_1(kr)\mathrm{d}k. \tag{B 6c}$$

Substituting the expressions above into equation (B 5), and interchanging order of integration leads to

$$\boldsymbol{L} = -\frac{32\boldsymbol{\Omega}}{3}\left(1 + \frac{3}{10}\mathrm{i}\lambda^2 + O(\lambda^3)\right) \tag{B 7}$$

where $\mathrm{Re}\{\mu a^3\boldsymbol{\Omega}\boldsymbol{L}\mathrm{e}^{\mathrm{i}\omega t}\}$ is the actual torque experienced by the oscillating disk.

A similar calculation may be used to determine the low-frequency correction for in-plane rotation of a disk, which was previously given by Kanwal (1970). We note that there is a sign error in Kanwal's expression since the first correction must be positive by (B 5) and the corresponding torque is given in table 1, entry c.

REFERENCES

Arkilic, E. B., Schmidt, M. A. & Breuer, K. S. 1995 Gaseous slip flow in long microchannels. *J. Microelectromechanical Syst.* **6**, 167–178.

Batchelor, G. K. 1967 *Introduction to Fluid Dynamics*. Cambridge University Press.

Brenner, H. 1964 The Stokes resistance of a slightly deformed sphere. *Chem. Engng Sci.* **19**, 519–539.

Bryzek, J., Peterson, K. & McCulley, W. 1994 Micromachines on the march. *IEEE Spectrum* **31**, 20–31.

Davis, A. M. J. 1993*a* Some asymmetric Stokes flows that are structurally similar. *Phys. Fluids* A **5**, 2086–2094.

Davis, A. M. J. 1993*b* A hydrodynamic model of the oscillating screen viscometer. *Phys. Fluids* A **5**, 2095–2103.

Faber, T. E. 1995 *Fluid Dynamics for Physicists*. Cambridge University Press.

Feuillebois, F. & Lasek, A. 1978 On the rotational historic term in non-stationary Stokes flow. *Q. J. Mech. Appl. Maths* **31**, 435–443.

Gatignol, R. 1983 The Faxén formulae for a rigid particle in an unsteady non-uniform Stokes flow. *J. Méc. Théor. Appl.* **1**, 143–160.

Gavze, E. 1990 The accelerated motion of rigid bodies in non-steady Stokes flow. *Intl J. Multiphase Flow* **16**, 153–166.

Happel, J. & Brenner, H. 1965 *Low Reynolds Number Hydrodynamics*. Prentice-Hall.

Hocquart, R. 1976 Régime instantané d'un liquide dans lequel un ellipsoïde de révolution tourne autour de son axe. *C. R. Acad. Sci. Paris* **283**, 1119–1122.

Hocquart, R. 1977 Régime instantané d'un liquide dans lequel un ellipsoïde de révolution tourne autour d'un axe équatorial. *C. R. Acad. Sci. Paris* **284**, 913–917.

Hocquart, R. & Hinch, E. J. 1983 The long-time tail of the angular-velocity autocorrelation function for a rigid Brownian particle of arbitrary centrally symmetric shape. *J. Fluid Mech.* **137**, 217–220.

Kanwal, R. P. 1964 Drag on an axially symmetric body vibrating slowly along its axis in a viscous fluid. *J. Fluid Mech.* **19**, 631–636.

Kanwal, R. P. 1970 Note on slow rotation or rotary oscillation of axisymmetric bodies in hydrodynamics and magnetohydrodynamics. *J. Fluid Mech.* **41**, 721–726.

Kim, S. & Karrila, S. J. 1991 *Microhydrodynamics* Butterworth-Heinemann.

Lai, R. Y. S. 1973 Translatory accelerating motion of a circular disk in a viscous fluid. *Appl. Sci. Res.* **27**, 440–450.

Lamb, H. 1932 *Hydrodynamics*, 6th edn. Dover.

Landau, L. D. & Lifshitz, E. M. 1959 *Fluid Mechanics*. Pergamon Press.

Lawrence, C. J. & Weinbaum, S. 1986 The force on an axisymmetric body in linearized time-dependent motion: a new memory term. *J. Fluid Mech.* **171**, 209–218.

Lawrence, C. J. & Weinbaum, S. 1988 The unsteady force on a body at low Reynolds number; the axisymmetric motion of a spheroid. *J. Fluid Mech.* **189**, 463–489.

Loewenberg, M. 1993*a* Stokes resistance, added mass, and Basset force for arbitrarily oriented, finite-length cylinders. *Phys. Fluids* A **5**, 765–767.

Loewenberg, M. 1993*b* The unsteady Stokes resistance of arbitrarily oriented finite-length cylinders. *Phys. Fluids* A **5**, 3004–3006.

Loewenberg, M. 1994*a* Axisymmetric unsteady Stokes flow past an oscillating finite-length cylinder. *J. Fluid Mech.* **265**, 265–288.

Loewenberg, M. 1994*b* Asymmetric, oscillatory motion of a finite-length cylinder: The macroscopic effect of particle edges. *Phys. Fluids* **6**, 1095–1107.

Loewenberg, M. 1994*c* Unsteady electrophoretic motion of a non-spherical colloidal particle in an oscillating electric field. *J. Fluid Mech.* **278**, 149–174.

Lovalenti, P. M. & Brady, J. F. 1993 The hydrodynamics force on a rigid particle undergoing arbitrary time-dependent motion at small Reynolds numbers. *J. Fluid Mech.* **256**, 561–605.

Lucas, S. K. 1995 Evaluating infinite integrals involving products of Bessel functions of arbitrary order. *J. Comput. Appl. Maths* **64**, 269–282.

Oberhettinger, F. & Badii, L. 1973 *Tables of Laplace Transforms*. Springer.

Pozrikidis, C. 1989*a* A singularity method for unsteady linearized flow. *Phys. Fluids* A **1**, 1508–1520.

Pozrikidis, C. 1989*b* A study of linearized oscillatory flow past particles by the boundary-integral method. *J. Fluid Mech.* **202**, 17–41.

Rallison, J. M. 1978 Note on the Faxen relations for a particle in Stokes flow. *J. Fluid Mech.* **88**, 529–533.

Smith, S. H. 1995 Structural changes in transient Stokes flows. *Q. J. Mech. Appl. Maths* **48**, 285–309.

Stokes, G. G. 1851 On the effect of the internal friction of fluids on the motion of pendulums. *Trans. Camb. Phil. Soc.* **9**, 8.

Tanzosh, J. P. & Stone, H. A. 1995 Transverse motion of a disc through a rotating fluid. *J. Fluid Mech.* **301**, 295–324.

Tanzosh, J. P. & Stone, H. A. 1996 A general approach for analyzing the arbitrary motion of a circular disk in a Stokes flow. *Chem. Engng Commun.* **150**, 333–346.

Tekasakul, P., Tompson, R. V. & Loyalka S. K. 1998 Rotatory oscillations of arbitrary axi-symmetric bodies in an axi-symmetric viscous flow: Numerical solutions. *Phys. Fluids* (to appear).

Tranter, C. J. 1966 *Integral Transforms in Mathematical Physics*. John Wiley & Sons.

Vedensky, D. & Ungarish, M. 1994 The motion generated by a slowly rising disk in an unbounded rotating fluid for arbitrary Taylor number. *J. Fluid Mech.* **262**, 1–26.

Vogel, S. 1994 Questions in fluid mechanics: Mixed mechanisms, complex shapes, and transitional regimes – help us decipher the devices of organisms. *Trans. ASME* I: *J. Fluids Engng* **116**, 195–196.

Williams, W. E. 1966 A note on slow vibrations in a viscous fluid. *J. Fluid Mech.* **25**, 589–590.